Origin, characteristics and distribution of fault-related and fracture-related dolomitization: Insights from Mississippian carbonates, Isle of Man

JAMES P. HENDRY*, JAY M. GREGG†, KEVIN L. SHELTON‡, IAN D. SOMERVILLE§
and STEPHEN F. CROWLEY¶
*Tullow Oil Limited, Number 1 Central Park, Leopardstown, Dublin 18, Ireland (E-mail: jim.hendry@tullowoil.com)
†Boone Pickens School of Geology, Oklahoma State University, Stillwater, OK 74078, USA
‡Department of Geological Sciences, University of Missouri, Columbia, MO 65211, USA
§School of Geological Sciences, University College Dublin, Belfield, Dublin 4, Ireland
¶School of Environmental Sciences, University of Liverpool, Liverpool L69 3GP, UK

ABSTRACT

Viséan limestones on the Isle of Man host numerous examples of fault-controlled and fracture-controlled dolomitization, which have been investigated to determine their macro-scale to micro-scale characteristics, geofluid origin, timing and relation to basin evolution. Geobodies composed of fabric destructive, ferroan, non-planar dolomite range from several centimetres to >300 m wide and tens to hundreds of metres long parallel to faults and/or fractures; they have sharply defined margins, cross-cut stratigraphy and locally finger out along beds or bed boundaries for tens of metres. Larger geobodies accompany NNE–SSW extensional faults with substantial breccia zones. One of these bodies hosts a sphalerite-rich breccia deposit cemented by dolomite. Saddle dolomite lines or fills vugs and fractures within dolomite geobodies, and is a minor late diagenetic phase in undolomitized limestones. Replacive dolomite has low matrix porosity owing to non-planar texture and associated cementation, and there is no evidence for subsequent leaching. Three dolomite stages are discriminated by texture, cathodoluminescence petrography and electron microscopy. Disseminated 'Dolomite 1' is substantially replaced and may be residual early diagenetic dolomite. Pervasive 'Dolomite 2' and 'Dolomite 3' have overlapping carbon–oxygen–strontium isotopic and fluid-inclusion characteristics that indicate precipitation from allochthonous, high-temperature (98 to 223°C) and high-salinity (15 to 24 wt% NaCl eq.) brines. These variably equilibrated with host limestones and mixed with resident pore fluids. Overlying mudrocks formed a seal for ascending fluids. Integration of data from the mineral deposit suggests that fault-fracture systems tapped different deep-seated fluid reservoirs at different temperatures, and implies fluid interactions with both metamorphic basement and sedimentary cover in large-scale circulation systems. This phenomenon probably took place during Mesozoic rifting, although an earlier event at the end of the Early Carboniferous cannot be discounted. In either case, a transient heat flow anomaly, previously unrecognized in the Irish Sea region, may be required to account for the hottest fluids.

Keywords Carboniferous, dolomitization, fluid inclusions, hydrothermal fluids, Irish Sea Basin, Isle of Man, stable isotopes, structural diagenesis.

INTRODUCTION

The importance of faults and fractures as either passive or active (syn-tectonic) conduits for fluid flow in sedimentary basins has gained increasing recognition in recent years, to the extent that 'structural diagenesis' is regarded as a key topic of research in the hydrocarbon and mineral resource industries (Laubach *et al.*, 2010). Faults are able to transmit deep-seated basin or basement-derived fluids into structurally higher and cooler strata, where they can interact with autochthonous formation fluids. The resultant thermal and/or chemical disequilibrium may lead to mineral authigenesis, dissolution, recrystallization, or some combination of processes. Where faults are passive fluid conduits, the fluid flux is typically controlled by geothermal convection or by tectonic loading and dewatering of deeply buried strata. Relatively enhanced permeabilities of fault damage zones focus upward fluid flow. The orientation of the faults (and associated fractures) to the regional strain field at the time may determine which orientations are 'open' to fluid flow and which are sealing. During active tectonism, fluid flow may be episodically driven through strain cycling in the deformation envelope or through release of overpressure build-up (Muir-Wood, 1994; Sibson, 1994). In either case, fluids can only migrate laterally away from the structural conduits on a macroscopic scale when they intersect permeable strata. Such permeability may be a result of favourable depositional facies (Grammer & Harrison, 2013), incomplete pore occlusion during earlier diagenesis or development of a joint or fracture network in otherwise tight rocks (e.g. López-Horgue *et al.*, 2010; Iriarte *et al.*, 2012). Pre-existing permeability is a prerequisite for diagenesis to occur from fault-sourced fluids, whether or not such fluids are under-saturated with respect to the host lithology.

One of the most striking manifestations of fault-related and fracture-related fluid flow is where it has caused fabric destructive dolomitization of limestone or replacement of pre-existing finely textured dolomite. Unlike most of the near-surface dolomitization processes that tend to form stratabound diagenetic geobodies, fault-related and fracture-related dolomites (FFRD) typically form geobodies that cross-cut stratigraphy and are geometrically constrained by tectonic fabrics. A subset of FFRD contains geochemical and fluid-inclusion evidence that the dolomitizing fluid was significantly hotter than the host strata at the time of dolomitization (e.g. Machel & Lonnee, 2002). These 'hydrothermal dolomites' have attracted much attention in the literature as potential petroleum reservoirs, and conceptual models have been proposed and invoked widely to predict their characteristics away from well control (e.g. Davies & Smith, 2006; Smith, 2006; Lavoie & Chi, 2010). The predictive value of these generic models is contentious, and it should be recognized that many of the numerous subsurface examples lack the specific structural relations that are inherent to these models. As a corollary, there are a limited number of outcrop examples where discrete dolomite geobodies linked to structural features have been described and characterized in detail. Such examples include those from NW Spain and SE Iran (López-Horgue *et al.*, 2010; Sharp *et al.*, 2010; Lapponi *et al.*, 2011; Dewit *et al.*, 2012). Other published examples frequently infer a tectonic or hydrothermal origin for dolomite bodies from stratigraphically discordant margins or geochemical characteristics.

This paper will provide a systematic field, petrographic and geochemical analysis of FFRD geobodies exposed on the coastal outcrop of Mississippian limestones on the Isle of Man, which is situated in the Irish Sea Basin between England and Ireland. Although the lack of mountainous terrain limits three-dimensional exposure of the geobodies, their two-dimensional relations, stratigraphic constraints, and relationships to faults and fractures are documented readily. The dolomitization is linked genetically to a recently discovered breccia-hosted Zn–Pb sulphide deposit within the outcrop area (Shelton *et al.*, 2011). By integrating textural and geochemical data from the mineral deposit and the more widespread FFRD geobodies, it is possible to demonstrate the role of allochthonous basement-involved fluids and thereby a direct tectonic control on dolomitization. Fluid sources, timing of dolomitization and implications of these results for prediction of FFRD petroleum reservoirs will be discussed.

GEOLOGICAL CONTEXT

The studied area consists of coastal outcrops of Viséan (Mississippian) platform carbonates in the south-east corner of the Isle of Man, near Castletown (Fig. 1A and B). Most exposures take the form of an extensive, *ca* 30 to 300 m wide, wave-cut platform, backed by low cliffs and

extending seaward through the intertidal zone. This shoreline exposure is present almost continuously from Cass-ny-Hawin (UK national grid reference SC 303696) to Kallow Point at Port St Mary (SC 207668), with the exception of sandy beaches in Derbyhaven Bay, Castletown Bay and Bay ny Carrickey. Strata are sub-horizontal or dip gently to the south-west, with localized low amplitude folding of probable Variscan origin (Fitches, 2011). Tournaisian polymict ferruginous conglomerates of the Langness Formation are exposed only on the Langness Peninsula, where they unconformably overlie Lower Ordovician metamorphosed turbidites of the Manx Group (Dickson *et al.*, 1987). The conglomerates represent syn-rift alluvial deposits and their deposition was followed by an early Viséan marine transgression and limestone deposition. The contact between Viséan limestones and the Manx Group phyllites at Cass-ny-Hawin is faulted, and other contacts are unexposed. Polyphase deformation and lower greenschist facies metamorphism of the Manx Group took place during the Acadian orogeny, and was accompanied by emplacement of several granitic intrusions (Fig. 1A). More details are given by Shelton *et al.* (2011) and references therein.

Lamplugh (1903) provided the first detailed geological analysis of the Isle of Man. The lithostratigraphy of exposed Mississippian carbonate strata was subsequently revised by Dickson *et al.* (1987), Chadwick *et al.* (2001) and, most recently, by Jackson *et al.* (2011) (Figs 2 and 3). In summary, the succession of roughly 360 to 400 m thickness spans the Arundian to Brigantian regional sub-stages of the Mississippian. It is dominated by variably fossiliferous platform limestones with typical open marine faunas dominated by crinoids, brachiopods, molluscs, foraminifera, bryozoa, ostracods and algae, with rare corals and goniatites. The Derbyhaven Formation represents a transgressive–regressive cycle through inner-ramp to mid-ramp depositional environments and contains cross-stratified oobioclastic grainstones (Turkeyland Member), tempestite packstones with argillaceous partings (Sandwick Member) and burrowed, silty argillaceous packstones (Skillicore Member). The overlying Knockrushen and Hodderense Limestone Formations are more offshore, mid to outer ramp deposits dominated by argillaceous wackestones and packstones; they are strongly bioturbated but storm-produced mega-ripples are present locally in the Knockrushen Formation.

The Balladoole Formation marks a change from a carbonate ramp to a steep-sided shelf, potentially related to the onset of glacio-eustasy in the Asbian (Chadwick *et al.*, 2001). It consists of shallow water grainstones and packstones that pass laterally and upwards into poorly stratified basinal calcareous mudrocks of the Bowland Shale Formation. At Poyllvaaish (SC 246675), the Bowland Shale Formation contains intercalated thin to medium bedded calciturbidites and debrites, plus 'olistoliths' of Waulsortian-type boundstone that are interpreted either to have been derived from gravitational collapse of an up-dip Balladoole platform margin (Dickson *et al.*, 1987), or from more localized syn-sedimentary faulting and slumping (Quirk *et al.*, 1990). An *in situ* Waulsortian-type mound is exposed in the walls of Cross Welkin Hill Quarry and is broadly similar in facies to coeval platform-edge bioherms of Ireland, North Wales and northern England (e.g. Somerville, 2003). A Late Viséan subcrop below Permo-Triassic cover in the north of the Isle of Man contains shallower mixed carbonate–siliciclastic facies than is typical for the Bowland Shale (Chadwick *et al.*, 2001). The stratigraphically highest part of the succession in the south-eastern Isle of Man is the Scarlett Volcanic Member. This part consists of a complex, slumped and brecciated assemblage of submarine volcaniclastic debris flows, basaltic pillow lavas and hemipelagic calcareous claystones of Brigantian age.

Viséan deposition in the central British Isles was characterized by extensional block and basin tectonics (e.g. Gawthorpe *et al.*, 1989). The Manx–Lakeland Ridge formed one such block, and is partially underpinned by the Acadian age Foxdale Granite (dated by Rb–Sr method at 383 ± 11 Ma; Chadwick *et al.*, 2001). This and other structural highs hosted extensive shallow carbonate environments, with deeper marine siliciclastic-dominated sedimentation in adjoining depocentres. On the Isle of Man, the Viséan syn-rift platform carbonates occupy an exhumed half-graben in the hanging wall of the Shag Rock Fault (Figs 1 and 3). This is one of several north-east/south-west trending structures regionally defining Carboniferous and Mesozoic depocentres, and which are probably Caledonian basement structures with long histories of reactivation (Quirk & Kimbell, 1997). Another is inferred offshore close to the Langness Peninsula. The regional stress field in the Early Carboniferous was oriented roughly NNW–SSE
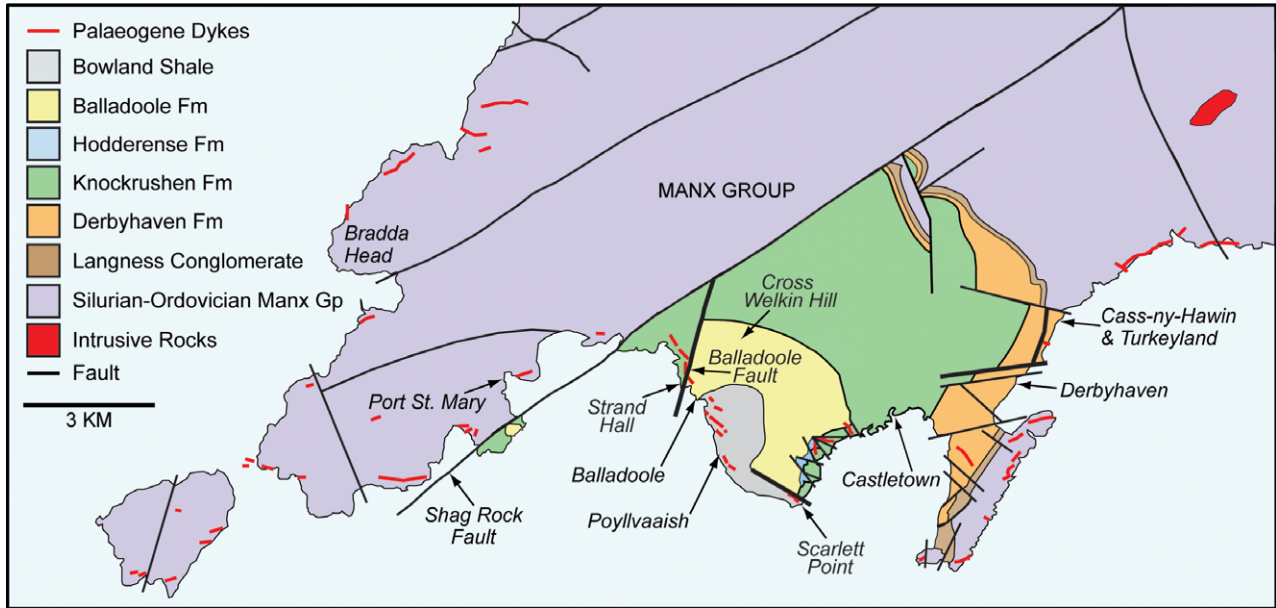
A
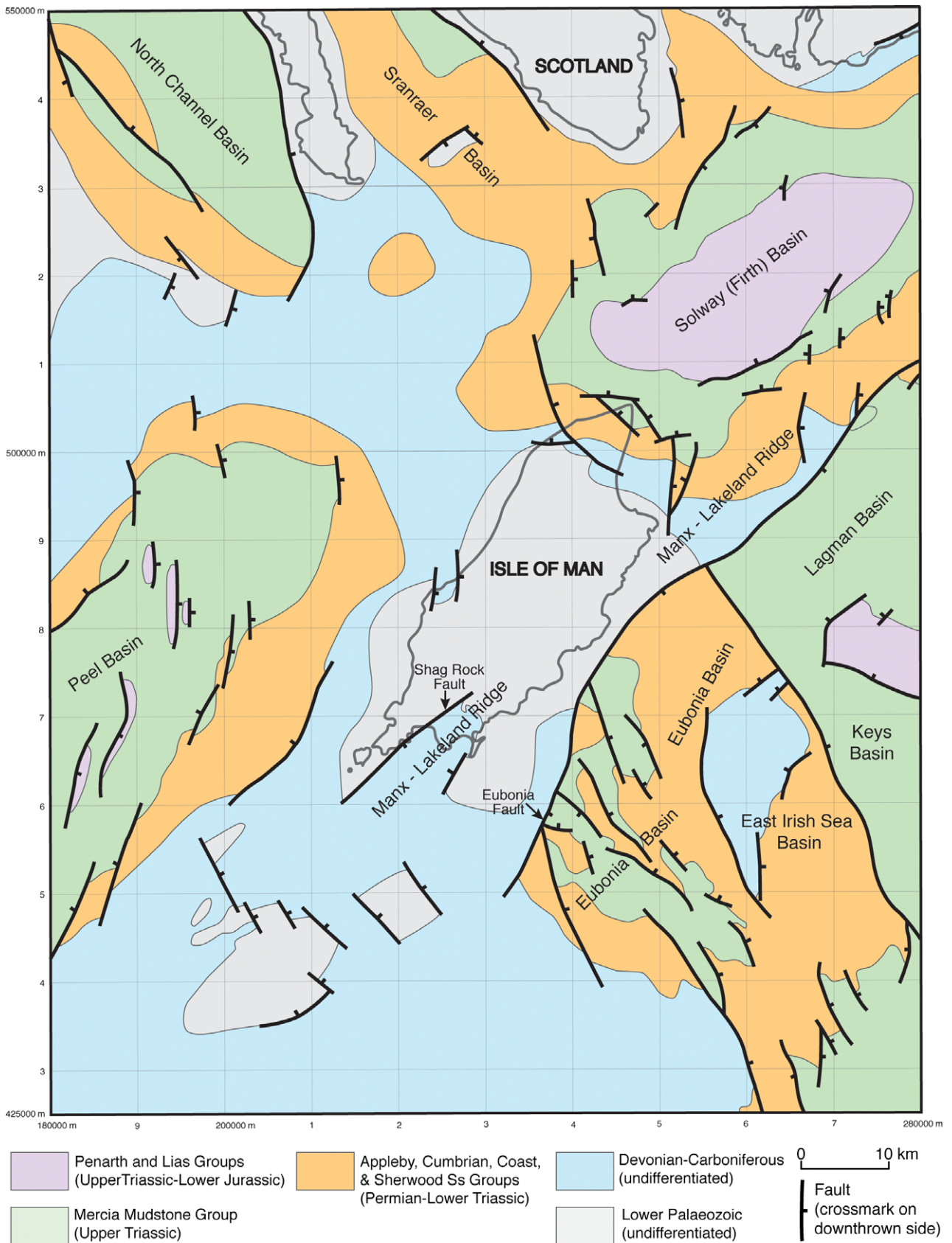
Fig. 1. (A) Simplified tectonic and outcrop/subcrop map of the Isle of Man and surrounding sedimentary basins (based on Chadwick *et al.*, 2001). The Manx–Lakeland ridge was a long-lived structural high and the offshore Eubonia and Peel basins were generated by Permo-Triassic rifting after the Variscan orogeny. (B) Detailed geology of the south-eastern part of the Isle of Man showing key sampling areas, faults and stratigraphic units. The faults with major dolomite geobodies are shown as thicker lines and the location of the sphalerite mineral deposit at Balladoole is indicated. Note that the Balladoole location is sometimes described in the literature as 'Salt Spring'.

Fig. 2. Summarized lithostratigraphic column, sedimentological characteristics and relative water depths for the Mississippian succession on the Isle of Man. Stratigraphic thicknesses are approximate or minimum values. The stratigraphic context of the Balladoole sphalerite deposit and ankerite veining in the mudrocks capping the limestone succession are indicated (see text for details).
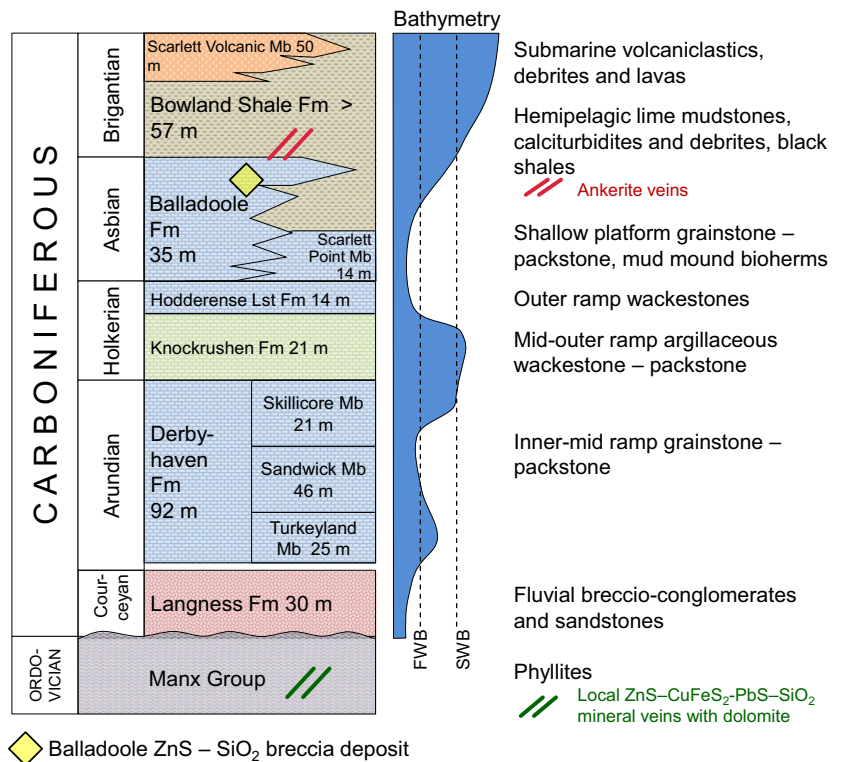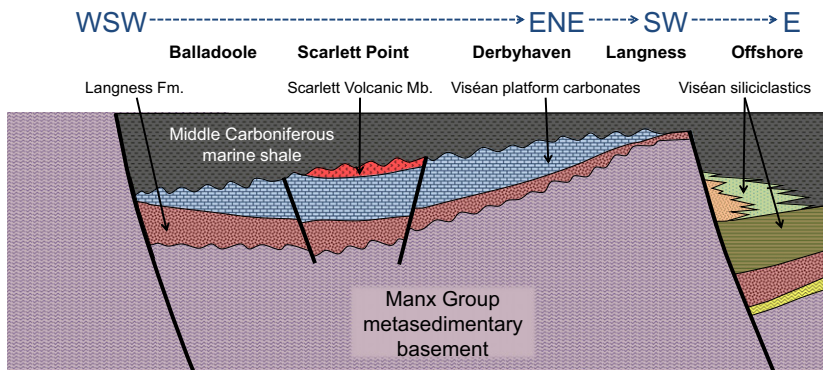
Fig. 3. Schematic cross-section of the study area showing tectonostratigraphic relations.

(Chadwick *et al.*, 2001) which suggests that there was some transtensional movement on the Shag Rock Fault and other similarly oriented structures. Syn-sedimentary fault activity is indicated by extensive slumping and sliding recorded in the Bowland Shale Formation. The fault trace is not exposed, but the NNE–SSW oriented Balladoole Fault adjacent to the Zn–Pb sulphide deposit described by Shelton *et al.* (2011) is probably linked to it (Fig. 1A and B). The WNW–ESE fault separating Viséan strata from the Manx Group at Cass-ny-Hawin has been interpreted as Early Carboniferous by Quirk *et al.* (2006), as have vertical east–west faults cutting the Viséan outcrop that show evidence of sinistral strike slip and that are interpreted as transverse faults that accommodated extension on the Shag Rock Fault.

The tectonic history of the south-eastern Isle of Man subsequent to the Mississippian is inferred from regional and especially offshore data (Quirk & Kimbell, 1997; Chadwick *et al.*, 2001; Fraser & Gawthorpe, 2003), and is summarized in Fig. 4. Post-rift thermal subsidence in the Late Carboniferous led to accumulation of >500 m of Namurian organic-rich mudrocks 10 km offshore in the Eubonia Basin (Fig. 1A). These form the primary source rock for Permo-Triassic East Irish Sea Basin hydrocarbon reservoirs (Hardman *et al.*, 1993). Namurian siliciclastics are present as subcrop in the north of the Isle of Man, and may formerly have been more widespread. Towards the end of the Carboniferous, WNW–ESE directed Variscan compression was partly accommodated on reactivated Early Carboniferous and Caledonide
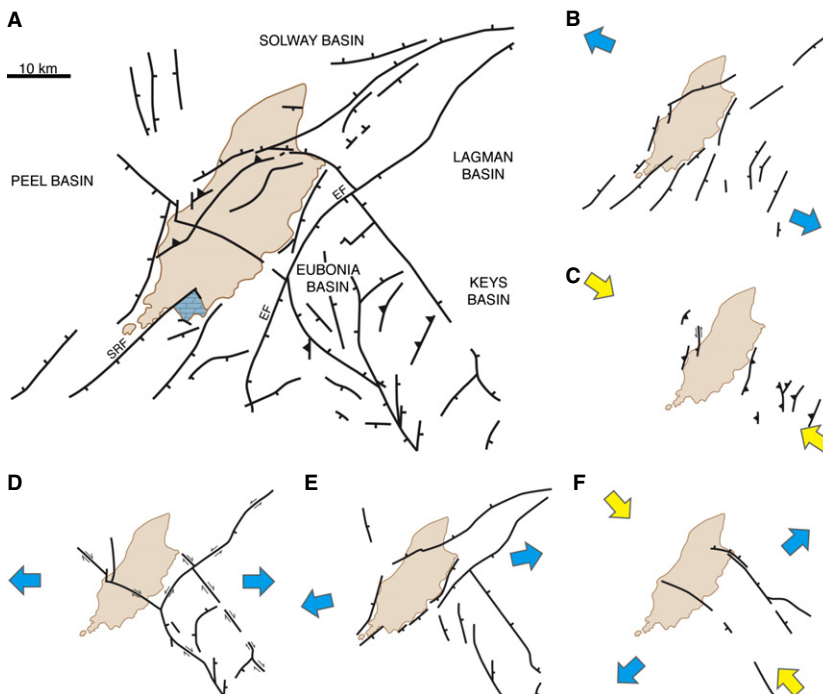
Fig. 4. Maps depicting the structural evolution of the Isle of Man and adjacent basins, in relation to the tectonic stress orientations (adapted from Quirk & Kimbell, 1997). (A) Present-day structural map showing the location of Viséan carbonate outcrop. (B) Early–Middle Carboniferous rifting. (C) Late Carboniferous (Variscan) compression. (D) Early Permian rifting. (E) Late Jurassic extension. (F) Palaeogene doming and extension.

faults. Inversion was common in offshore basins to the north and west of the Isle of Man, while to the east and south, there is evidence of local fault reactivation and uplift episodes, including substantial reverse displacement on the Eubonia Fault (Fig. 1A). Thick Namurian and Westphalian successions are preserved in major offshore depocentres, but it is likely that several hundred metres of Pennsylvanian overburden were removed from the study area (Chadwick *et al.*, 2001). In the Late Permian to Early Triassic, rifting in offshore basins resulted from east–west directed extensional stresses associated with the break-up of Pangaea. The Manx–Lakeland Ridge remained a structurally elevated feature and faulting took place on new or inherited (Caledonian to Variscan) north–south to NNW–SSE trending structures, accompanied by reactivation of major Early Carboniferous NNE–SSW oriented rift structures (Needham & Morgan, 1997). Jurassic and Cretaceous post-rift thermal extension was probably punctuated by an episode of renewed rifting in the Late Jurassic (Quirk & Kimbell, 1997). However, much of the evidence has been obliterated by Palaeogene uplift associated with thermal doming, as part of the continued North Atlantic opening, and by Neogene erosion. Apatite fission track data suggest that up to 1 km of overburden was eroded away from the southern part of the Isle of Man at this time (Green *et al.*, 1997; Chadwick *et al.*, 2001).

As well as the Balladoole Fault, several other important faults cut the Viséan crop out in the study area. These are oriented mostly WNW–ESE or WSW–ENE (Fig. 1B). Smaller scale fractures also follow these trends, but an additional set has a north-west/south-east orientation. Fractures are mostly sub-vertical and show centimetre-scale offsets. Fault plane dips are difficult to constrain other than in quarries, where they are also very steep ≥80°. Fault throw is also difficult to determine with limited 3D exposure. A maximum of several tens of metres is likely, based on the lithostratigraphy, with the exception of the Shag Rock Fault, where the net vertical displacement is probably >100 m.

SAMPLING AND METHODS

A total of 140 specimens were collected from localities listed in Table S1 during field campaigns in 2004, 2007 and 2009, and their positions were recorded by GPS and plotted onto Google Earth imagery. Field photographs were also indexed with GPS coordinates. A majority of the rock samples were collected from the coastal outcrop. Inland exposure of the carbonates is rare, with the exception of a large working quarry at Turkeyland (SC 295690) and smaller abandoned quarries at Cross Welkin Hill (SC 246687), Balladoole (SC 245682) and Poyllvaaish (SC 675247; the 'Black Marble Quarry'). Sampling was focused on fault-related and fracture-related dolomite bodies and adjacent limestones. The former are usually very distinctive in the field, but mineralogical identifications were verified using alizarin red-S in 2% HCl on freshly broken rock surfaces.

The data set includes seven specimens from a dolomite-cemented Zn–Pb sulphide breccia deposit on the lower foreshore at Balladoole (SC 243679) described by Shelton *et al.* (2011) and seven mineralized veins from the Manx Group in the abandoned Bradda Head and Foxdale mining areas. It also includes several dolomite samples from the wave-cut platform at Ronaldsway (SC 295686). These samples were obtained during earlier visits, and this part of the exposure has since been obscured by a seaward extension of the airport runway (in 2008).

Full details of sample preparation and analytical methods are provided in the Online Supplementary Information for this paper. Rock samples were slabbed and prepared for petrographic examination as highly polished thin sections and acetate peels from polished, alizarin red-S and potassium ferricyanide stained slabs. Thin sections were examined by conventional optical microscopy and cathodoluminescence (CL) microscopy. A representative subset was studied using backscatter mode scanning electron microscopy (BSEM). Many samples were also observed using ultra-violet epifluorescence to look for hydrocarbon inclusions, although none were found.

Fluid inclusion microthermometry was carried out on selected dolomite, calcite, quartz and sphalerite specimens, extending and re-evaluating the initial data set collected by Shelton *et al.* (2011). Care was taken to analyse primary or pseudo-secondary inclusions based on careful petrography, including distribution within crystals and consistent size and liquid: vapour ratios (Goldstein & Reynolds, 1994). Homogenization temperatures (T_h) and last ice melting temperatures (T_m) are reproducible to ±2°C and $\pm0\cdot2$°C, respectively. No pressure corrections were made to T_h data, because it was not possible to unambiguously determine burial depth at the time(s) of precipitation.

A total of 238 powder samples for stable isotope ratio measurement by conventional acid digestion were micro-drilled from thin section counterparts under a binocular microscope. Full analytical results are provided in Table S2. Average precision from repeat analyses of selected samples was better than ±0·1‰ for carbon and oxygen, and raw data were standardized to NBS-19. In order to calculate precipitation temperatures and fluid $\delta^{18}O$ compositions, the equilibrium oxygen isotope fractionation of Sheppard & Schwarcz (1970) was used for dolomite and ferroan dolomite or ankerite, and that of Friedman & O'Neil (1977) was used for calcite.

Splits from 34 of the sample powders were also analysed for strontium isotopes using conventional preparation techniques and thermal ionization mass spectrometry (TIMS). Analytical precision was monitored by repeated analysis of NBS-987 and is better than ±0·000014 at 95% confidence interval. Results are presented in Table S2. All measured $^{87}Sr/^{86}Sr$ data have been normalized to the NBS-987 value of 0·710248 (McArthur *et al.*, 2000). Precision on total Sr concentrations is better than ±10 ppm.

A small number of dolomite sample powders (16) were verified for mineralogical purity using standard powder X-ray diffractometry (XRD) and their major and trace element composition was then determined by inductively coupled plasma mass spectrometry (ICP-MS; results in Table S3). Precision and accuracy for the latter are estimated at better than ±5%, based on replicate analyses and certified reference material analytical results.
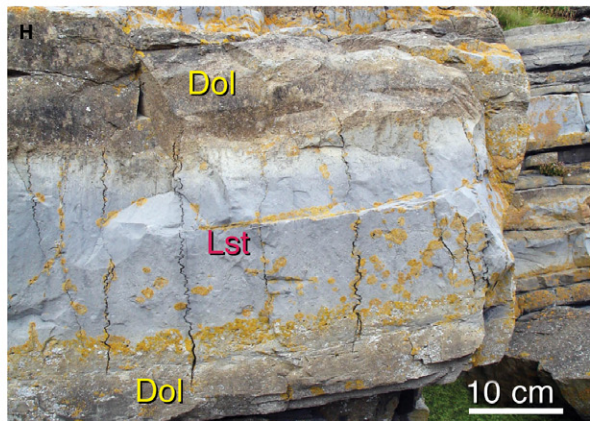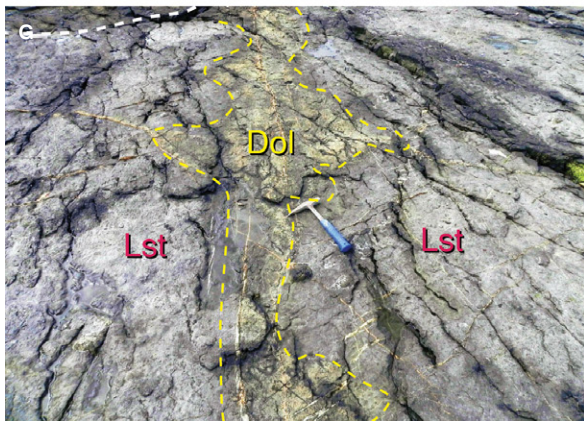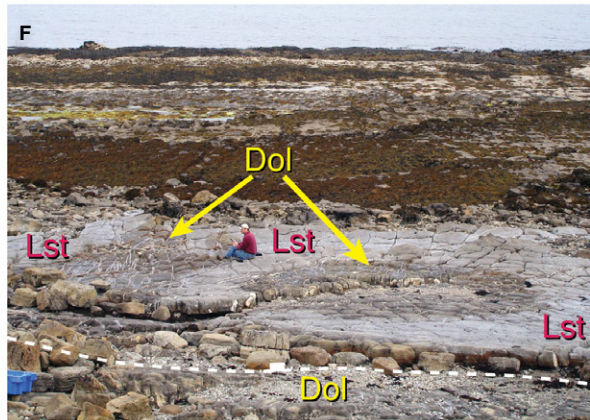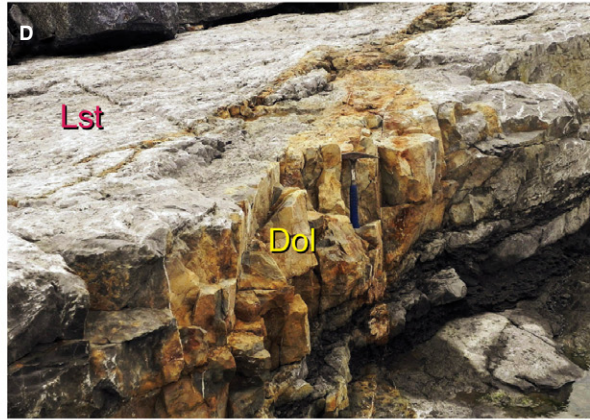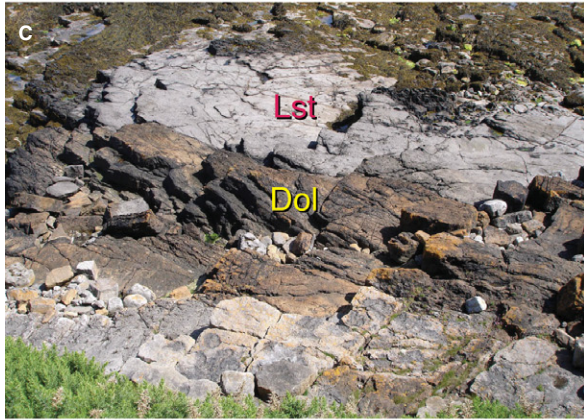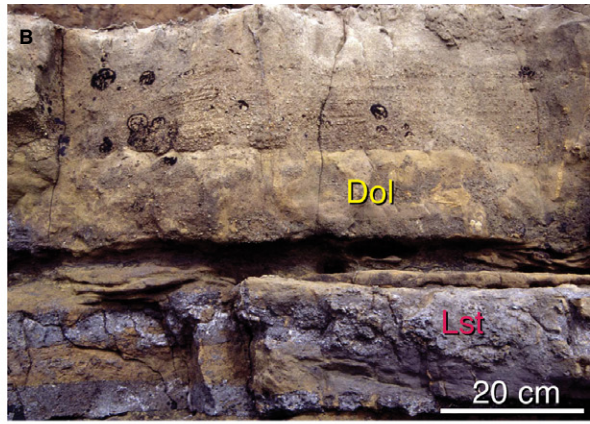
FIELD RELATIONS

Fault-related and fracture-related dolomite geobodies are present in all of the studied formations and are distinguished easily at outcrop by their brown to reddish-brown weathered appearance compared to the medium to dark grey of the surrounding limestones. The colour difference is also present on fresh surfaces, albeit more subtle. Based on petrographic observations (below), limestones may contain up to about 10% of disseminated dolomite, but the dolomite samples contain no relic limestone and only minor late stage calcite cements associated with dedolomitization. In contrast, Dickson & Barber (1977) recorded substantial metre-scale mineralogical heterogeneity in a single dolomitized bed in Derbyhaven Bay. This bed has now been partly obscured by the airport runway extension, but observations confirm a more gradational colour variation along what remains of this bed than is typical of the section. However, little evidence for partial dolomitization has been encountered from more geographically and stratigraphically widespread analyses.

Exposed dolomite geobodies vary widely in size and shape but share some common characteristics, such as spatial relation to faults and fractures, tendency to cut across stratigraphy, colour and rough or jagged weathered surfaces compared to limestones (Figs 5 to 7). Areally, the largest geobodies are associated with the NNE–SSW Balladoole Fault and the parallel fault that extends from Cass-ny-Hawin into Derbyhaven Bay (Fig. 1B). These geobodies are at least 100 m and *ca* 350 m wide, respectively; their absolute thickness cannot be determined owing to the limited 3D exposure and gentle regional dip, but in the east side of Turkeyland Quarry, dolomitization is present through the exposed, *ca* 20 m section of the Derbyhaven Formation. In smaller examples, dolomite extends from several metres to *ca* 30 m laterally away from faults. The partially dolomitized bed studied by Dickson & Barber (1977) contained 30 to

Fig. 5. Field relations and characteristics of dolomite bodies; see Fig. 1B for locations. (A) Balladoole dolomite body exposed at low tide, close to the sphalerite breccia deposit of Shelton *et al.* (2011). Dolomite weathers orange-brown and limestone grey. (B) Dolomite replacement of cross-bedded grainstone, Derbyhaven Formation, Derbyhaven. (C) Cross-cutting, 3 m wide dolomite body in grain/packstones close to north–south fault, Derbyhaven Formation, Cass-ny-Hawin. (D) Narrow (0·3 to 0·8 m) fracture-related dolomite body cutting Derbyhaven Formation packstones, Derbyhaven. (E) Balladoole Fault (white dashed line), Balladoole Formation grainstones on the hangingwall (right) are dolomitized, Knockrushen Formation wackestones on the footwall (left) are only dolomitized adjacent to fractures and locally within about 1 m of the fault plane. Persons for scale are *ca* 1·8 m tall. (F) Brown-weathering haloes of dolomitized wackestone surrounding fractures in hangingwall. Grain/packstones on the footwall of the fault (white dashed line) are fully dolomitized. Derbyhaven Formation, Cass-ny-Hawin. Arrows show location of Fig. 6C. (G) Grey-brown dolomitization halo up to 1·2 m wide surrounding dolomite-filled fracture in Knockrushen Formation wackestones, about 3 m from the Balladoole Fault, Strand Hall. Hammer is 40 cm long (H) Dolomitization along gently inclined bed boundaries of Knockrushen Formation wackestones, hangingwall of the ESE–WNW fault at Scarlett Point. See Fig. 6F for context.
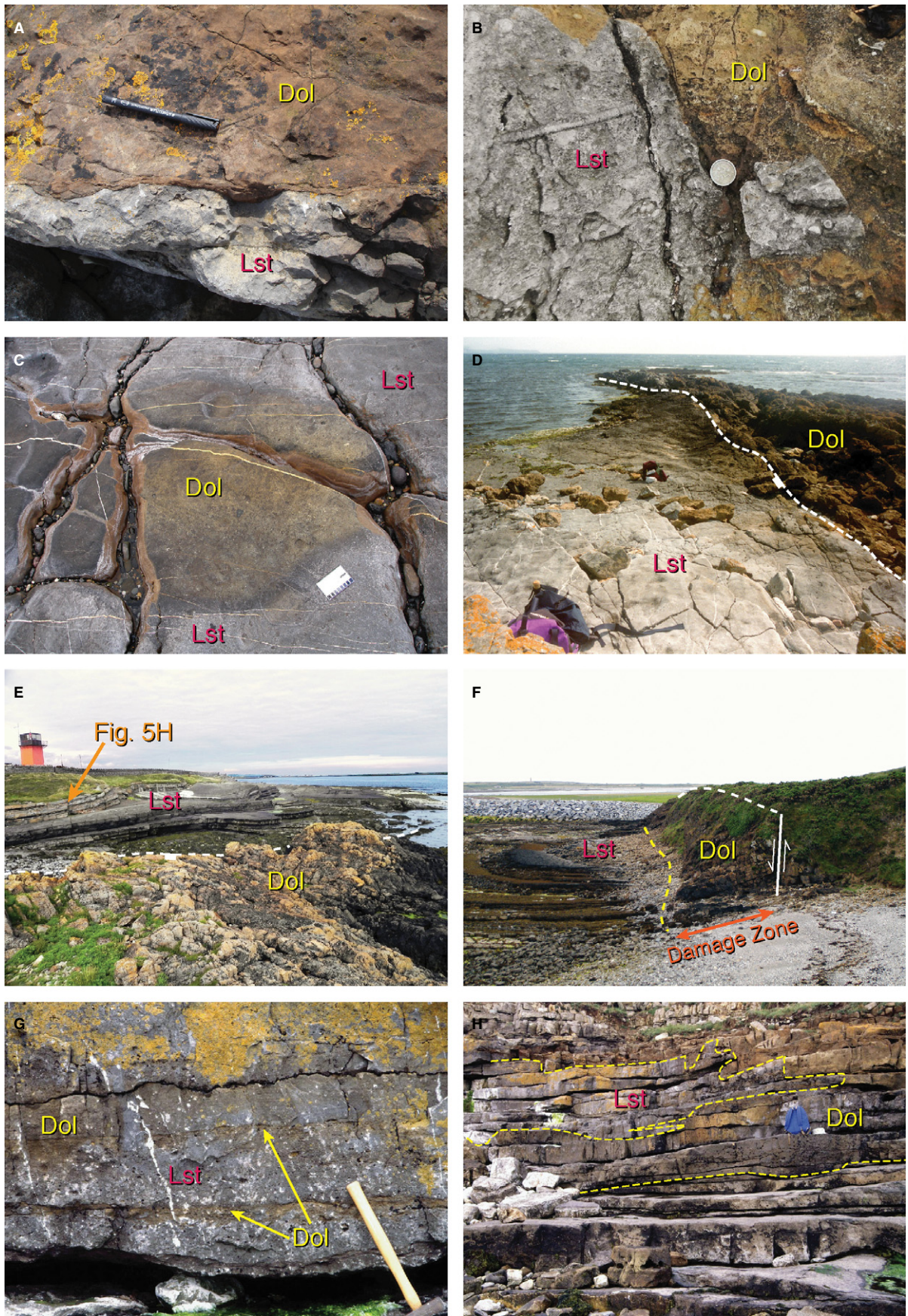
Fig. 6. Field relations and characteristics of dolomite bodies; see Fig. 1B for localities. (A) Typically sharp margin of cross-cutting dolomite body in Derbyhaven Formation grainstones, Cass-ny-Hawin. Pen is 15 cm long. (B) Sharp, partially fracture-constrained margin of dolomite in Balladoole Formation packstones, Balladoole. Coin is 2·5 cm wide. (C) Diffuse margin of fracture-related dolomite halo in wackestones (see Fig. 5F), Derbyhaven Formation, Cass-ny-Hawin. Card is 10 cm long. (D) ENE–WSW fault (white dashed line) within the Derbyhaven Formation at Derbyhaven. Coarse grainstones on the footwall (right) are pervasively dolomitized, while interbedded pack/grainstones on the hangingwall (left) are predominantly limestones, albeit with partial dolomitization in some beds (Dickson & Barber, 1977). Rucksack is *ca* 30 cm wide. (E) View north across ESE–WSW fault at Scarlett Point (white dashed line), in the foreground are pervasively dolomitized grainstones of the Bowland Shale Formation, and in the background are partially dolomitized wackestones of the Knockrushen Formation overlying undolomitized argillaceous mudstones of the Hodderense Formation. Arrow shows location of Fig. 5H. Field of view in the middle ground is *ca* 100 m. (F) View along north–south fault in the Derbyhaven Formation at Cass-ny-Hawin. Dolomitization is pervasive in the fault damage zone and proximal footwall, but dissipates over 5 to 10 m into the hangingwall limestones. Pervasive dolomite is present at the same level in Turkeyland Quarry, about 150 m to the west (right) of the photograph. (G) Dolomite 'fingering' along beds in grain/packstones on the hangingwall of the fault in (F). Hammer is 40 cm long. (H) Partial dolomitization in packstones at the lateral margin of a fault-constrained dolomite body, Derbyhaven Formation, Derbyhaven. Rucksack is *ca* 30 cm wide.

100% dolomite for *ca* 180 to 210 m away from a major fault.

Dolomite geobodies of tens to ≥100 m width tend to be hosted in grainstone and packstone lithologies (Fig. 5A and B), and dolomite extends laterally further from faults in grainier beds than in muddy ones. Cross-cutting dolomite 'dyke-like bodies' are associated with fractures in Derbyhaven Formation grainstones between Derbyhaven and Cass-ny-Hawin, and are up to 3 m across (Fig. 5C and D). Within mudstones and wackestones, the geobodies tend to extend no more than 1 dm to 1 to 2 m away from the faults (Fig. 5E). 'Haloes' of dolomite commonly extend outwards from dolomitic fractures and veins in the Knockrushen Formation at Derbyhaven Bay and Strand Hall, but only for several centimetres to *ca* 0·5 m (Fig. 5F and G). In the Hodderense Formation at Scarlett Point, dolomitization extends along the limestone bed boundaries but rarely penetrates entirely through the individual beds (Fig. 5H).

The margins of cross-cutting dolomite geobodies are almost always sharp and are straight to moderately undulating. In grainstones and packstones, this dolomite to limestone transition is on a millimetre to centimetre-scale (Fig. 6A and B). In wackestones and mudstones, and especially in dolomite 'haloes' around fractures, the transition can grade over several centimetres (Figs 5G and 6C). Dolomite geobodies can end abruptly at cross-cutting joints or calcite veins, but other sharp contacts have no clear visible control. In several cases, the dolomite to limestone transition is defined by a fault (for example, at Scarlett Point and at Strand Hall, Fig. 6D and E). This observation raises the possibility of structurally offset stratabound geobodies as opposed to dolomitization being related genetically to faulting. However, these dolomites usually discontinue and/or cut across bed boundaries if tracked along individual beds away from the surface fault trace. Moreover, the fault damage zone is invariably dolomitized (Fig. 6F), and dolomite fracture 'haloes' or metre-scale dolomite geobodies are commonly present on the limestone side (typically the footwall) of the faults (for example, Fig. 5F). Where dolomite extends out along beds of grainstone laterally away from faults, its transition to limestone is more gradual (Fig. 6G and H).

Dolomite geobodies and fault damage zones are cut locally by veins of coarse white to yellowish-pink saddle dolomite, and saddle dolomite locally fills moulds of gastropods and bivalves (Fig. 7A) in both dolomitized and undolomitized limestones. Veining is locally intense within several metres on each side of fault planes, and several episodes of opening and cementation may be discerned. Saddle dolomite veins locally penetrate into undolomitized limestones, but most limestone-hosted veins are plugged by white sparry calcite.

Two significant breccia zones are present in the studied outcrop; the most extensive hosts the sphalerite breccia deposit at Balladoole, and is probably related to a splay extending from the Balladoole Fault. A second is present at Derbyhaven Bay, where it marks the trace of a dolomite-associated NNE–SSW fault. Both breccias contain rounded and embayed dolomitized limestone clasts, and both are cemented extensively by white to pink sparry saddle dolomite with additional saddle dolomite in cross-cutting veins (Fig. 7B). At Balladoole, the clasts are also rimmed by up to 1 cm of sphalerite, quartz and minor galena (Fig. 7C; and see fig. 8 in Shelton *et al.*, 2011). Dolomite veins cross-cutting lime-
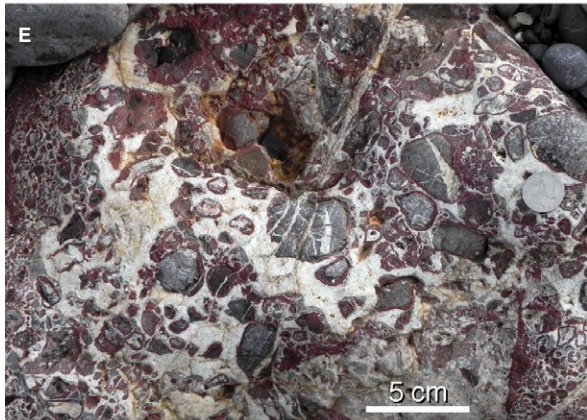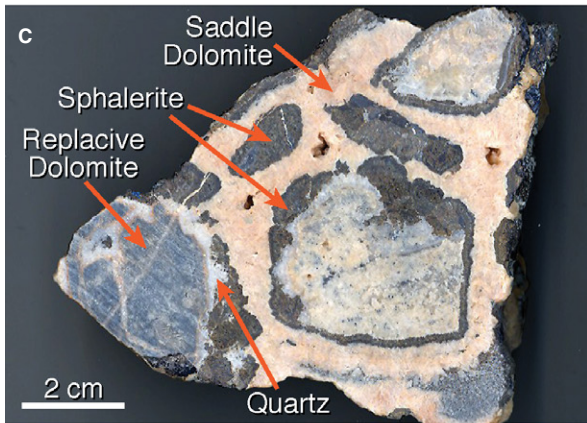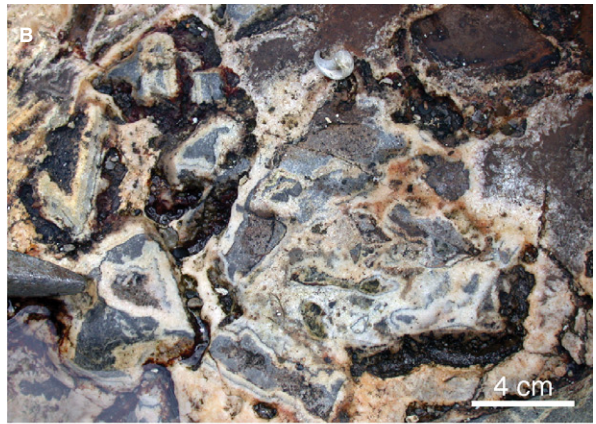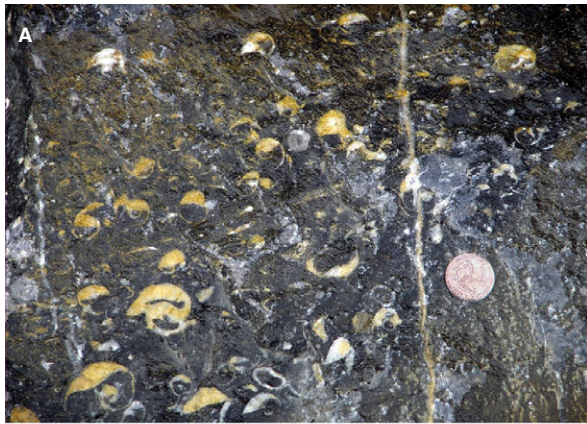
Fig. 7. Field relations and characteristics of dolomite bodies; see Fig. 1B for locations. (A) Dolomitized grainstones with saddle dolomite cement filling biomoulds and geopetal voids, Derbyhaven Formation, Turkeyland Quarry. Coin is 2·5 cm wide. (B) Breccia-related vugs in replacive dolomite lined by white saddle dolomite cement, Balladoole Formation, Balladoole. (C) Sawn slab of mineralized dolomitic breccia from the Balladoole mineral deposit. Clasts are rimmed by sphalerite and quartz and cemented by pink saddle dolomite. (D) Saddle dolomite (white) – sphalerite (brown) – galena (grey) in vein cutting Knockrushen Formation wackestones, Castletown. Coin is 2·5 cm wide. (E) Breccia in fault damage zone associated with north–south fault at Cass-ny-Hawin. Rounded dolomite clasts are mantled by hematite and cemented by coarse saddle dolomite. (F) Saddle dolomite (white) veins with associated hematite (red) cutting Derbyhaven Formation limestones at Derbyhaven. Coin is 2·5 cm wide. (G) Vugs of <5 cm to approximately 50 cm wide (arrows) developed in grainstone beds *ca* 5 m along strike from a fault, Derbyhaven Formation, Turkeyland Quarry. (H) Detail of saddle dolomite cement lining vugs in (G), brown colour reflects fine-scale replacement by calcite and Fe-oxide. Coin is 2·5 cm wide.

stones at Castletown also contain minor sphalerite and galena (Fig. 7D). Breccia clasts at Derbyhaven have millimetre to centimetre rims of hematite (Fig. 7E; Crowley *et al.*, 2013), and some saddle dolomite veins cutting dolomite geobodies at Derbyhaven and in the adjacent Turkeyland Quarry also contain a narrow red hematite zone (Fig. 7F).

Vuggy porosity is locally present within dolomite geobodies, typically associated with veins and breccias and rarely with solution-enlarged biomoulds. The vugs are typically *ca* 1 to 10 cm in diameter, but in Turkeyland Quarry a series of larger vugs (up to 0·5 m across) extends along a bedding plane in dolomitized grainstones close to a fault (Fig. 7G). Vugs are lined by coarse saddle dolomite, which is white to pale pink where fresh, and dark brown owing to

included Fe-oxides where substantially dedolomitized (Fig. 7H). Other than the vugs and scattered incompletely filled biomoulds, there is no visible porosity in the geobodies. Well-developed 'zebra' dolomites, a conspicuous feature of many hydrothermal dolomites, have not been observed on the Isle of Man.

Calcareous claystones of the Bowland Shale Formation on the foreshore and in the adjacent small quarry at Poyllvaaish contain minor <2 cm wide dolomite veins which are dissected by a major set of regularly spaced, east–west trending saddle ankerite-calcite veins (Fig. 8A and B). These are 1 to 10 cm wide, parallel sided, vertical and straight, but with local en échelon segments, relays and blind terminations. They infrequently contain angular wall-rock fragments, with more intense wall-rock brecciation
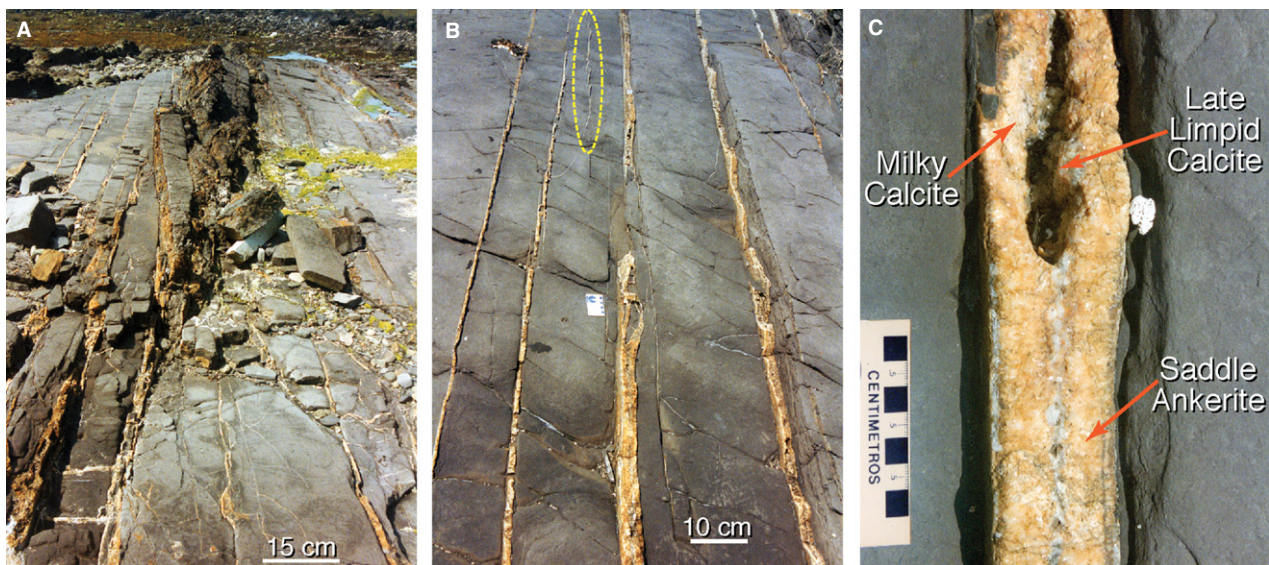
Fig. 8. (A) Field photograph of east–west trending ankerite-calcite veins dissecting calcareous mudrocks of the Bowland Shale Formation at Poyllvaaish. (B) Detail of ankerite-calcite veins showing blind terminations and en-echelon splays (highlighted). (C) Close-up of incompletely filled vein with saddle ankerite and late limpid calcite cements.

where veins intersect. The saddle ankerite cement is coarsely crystalline and salmon pink in colour, weathering to yellow-orange (Fig. 8C). It contains rare millimetre-size pyrite and sphalerite crystals (for example, fig. 6 in Shelton *et al.*, 2011), but is otherwise texturally similar to saddle dolomite which lines vugs and cement breccias in the large dolomite geobodies. Subsequent calcite is milky white and very coarsely crystalline. Minor limpid calcite cement is present locally in the centre of incompletely filled veins (Fig. 8C).

Palaeogene dolerite dykes locally cut across the onshore Viséan succession with a west–east to north-west/south-east trend (Fig. 1B) and are associated with the Northern Irish magmatic centre of the North Atlantic Large Igneous Province (Saunders *et al.*, 1997). These dykes show no spatial or geometrical relation to the dolomite geobodies. Ankerite veins at Poyllvaaish are cut by one such dyke and show some recrystallization and discolouration (from pink to grey) within *ca* 2·5 m of the intrusion. There is also no systematic relation of dolomitization to igneous rocks of the Scarlett Volcanic Member. The volcanic rocks are locally juxtaposed against dolomite at Scarlett Point, but elsewhere they overlie and contain interbeds and rafted blocks of undolomitized limestone (Dickson *et al.*, 1987).

RESULTS

Petrography, mineralogy and paragenesis

A detailed diagenetic study of the undolomitized Viséan limestones is beyond the scope of this paper. Some general information was provided by Dickson *et al.* (1987) while the diagenesis and geochemistry of the Derbyhaven Formation was specifically addressed by Dickson & Coleman (1980). Radiaxial fibrous marine cements have been observed in samples of Balladoole Formation mud-mound facies collected for this study, and early diagenetic calcite–silica concretions are present in the Knockrushen and Hodderense Limestone Formations (Dickson & Barber, 1976) but other macroscopic syndepositional precipitates are rare. The most abundant pore-filling cement is non-ferroan to zoned ferroan, equant and syntaxial sparry calcite that is moderate to dull orange-brown in CL. Centimetre-amplitude stylolites and dissolution seams are present locally through the succession (Fitches, 2011), in places marking bed boundaries.

Several generations of fracturing and calcite cementation can be identified in the limestones. The rarity of calcite-filled fractures in dolomite geobodies suggests that most (but not all) of these pre-dated dolomitization.

Dolomitization is pervasive within the sampled geobodies and is remarkably consistent in character (for example, Fig. 9A and B). Replacive dolomite is fine to medium crystalline (10 to 50 μm) and turbid, with planar-s to non-planar textures (*sensu* Sibley & Gregg, 1987). It commonly displays undulatory extinction. Where present, the small amount of intercrystalline space is typically filled by clay minerals, Fe-oxide and/or pyrite (especially in dolomitized wackestones and mudstones). In general terms, muddy limestones are replaced by finer crystalline dolomite than are grainy limestones, and dolomite crystals in the latter commonly have relatively limpid rims around inclusion-rich centres. There is little detailed fabric retention, although it is common for calcitic bioclasts such as crinoid and brachiopod fragments to be replaced by one or more anhedral dolomite crystals that are significantly coarser than the mode of the sample (Fig. 9C). These crudely replaced bioclasts may show partial silicification that probably pre-dated dolomitization. In rare cases, they are preserved with their original calcitic mineralogy. Micritic limestones close to the geobodies may contain several per cent of disseminated finely crystalline planar-e or planar-s dolomite.

Saddle dolomite cement is medium to very coarsely crystalline (50 to 1000 μm; up to 5000 μm in some veins), with characteristic curved crystal faces as well as sweeping extinction (for example, Fig. 9D). It is less turbid than replacive dolomites but still contains abundant fluid and solid (mostly Fe-oxide) inclusions that are concentrated locally along growth zones. Partly dedolomitized crystals contain more Fe-oxide, non-ferroan calcite and porosity. These are either concentrated into growth zones or follow a latticework pattern defined by growth zones and cleavage traces (Fig. 9E). The Fe-oxide content is locally sufficient to make the crystals opaque. Saddle dolomite is also present as a late stage void-filling and vein-filling cement in some undolomitized limestones, particularly in the Derbyhaven and Turkeyland areas.

X-ray diffractometry does not reveal any consistent differences between replacive dolomites and saddle dolomite cement. The (104) peak positions are all <0·2886 nm of ideal dolomite.
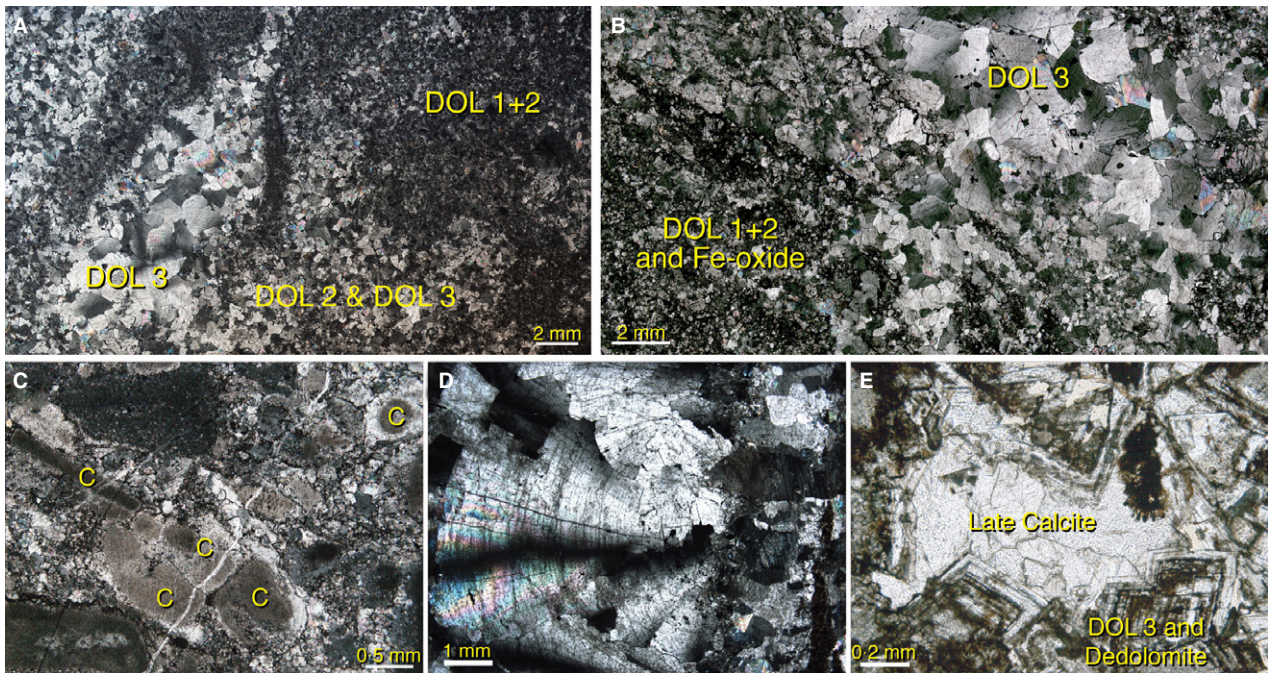
Fig. 9. Photomicrographs showing fabrics and textures of dolomitized limestones. All between crossed polarizers except (E). (A) Fine crystalline matrix-replacive DOL 1+2, medium crystalline DOL 2 (probably replacing grainstone), and coarse void-filling saddle DOL 3 cement. Bowland Shale Formation, Scarlett Point, 2 mm scale. (B) Dolomitized packstone replaced by DOL 1+2, with saddle DOL 3 cement filling vein. Dedolomitization is responsible for the opaque Fe-oxide between the replacive crystals. Derbyhaven Formation, Cass-ny-Hawin, 2 mm scale. (C) Dolomitized grainstone with many crinoid grains (C) replaced by single anhedral dolomite crystals, Derbyhaven Formation, Cass-ny-Hawin, 0·5 mm scale. (D) Saddle dolomite cement filling vein, Bowland Shale Formation, Poyllvaaish, 1 mm scale. (E) Saddle DOL 3 and subsequent equant calcite, brown zones in DOL 3 indicate fine-scale replacement by Fe-oxide and calcite (incipient dedolomitization), Balladoole Formation, Balladoole, 0·2 mm scale.

Principal ordering peaks (101), (015) and (021) (Goldsmith & Graf, 1958) are present, but the (015) peak is attenuated relative to the (110) peak indicating some degree of disorder, which is consistent with a calcian and ferroan composition.

Three distinct stages of dolomite can be recognized using CL and BSEM, allowing a paragenesis to be established (Figs 10 and 11). Dolomite 1 (DOL 1) and Dolomite 2 (DOL 2) are replacive, and Dolomite 3 (DOL 3) is pore-filling cement in vugs and fractures. Dolomite 1 consists of disseminated 5 to 20 μm cores of coarser anhedral crystals within some geobodies, as well as patchily distributed dolomite crystals within adjacent limestones. Its CL properties vary from dull to medium red and unzoned, to strongly zoned bright and very dark red, frequently with corrosion textures and partial replacement by very dark brown to non-CL DOL 2 (Fig. 10A to D). Precise zoning patterns vary among localities and are best preserved in the limestone-hosted crystals (Fig. 10E). Rarely, DOL 1 is partially

to severely replaced by CL-zoned calcite and Fe-oxide (Fig. 10F).

Dolomite 2 accounts for the majority of the replacive dolomite within the geobodies, and it overgrows DOL 1 where present. It is very dark brown to non-CL (Fig. 10B to D and F) and stains with potassium ferricyanide, confirming an iron-rich composition. Mottling in BSEM corresponds to the presence of less ferroan DOL 1 cores and of silt or clay inclusions, otherwise DOL 2 appears relatively homogeneous on a thin section scale.

Dolomite 3 corresponds to the saddle dolomite cement, and it probably also occupies some intercrystalline space within non-planar DOL 2 mosaics and/or partially replaces DOL 2. Boundaries between DOL 2 and DOL 3 are sharp where the latter fills fractures and well-defined vugs, but more gradational in some other cases. It is ferroan to locally ankeritic (3 to 15 mol% $FeCO_3$) and slightly calcium-enriched compared to stoichiometric dolomite (Fig. 12A). Crystals are uniformly non-CL, with the exception of
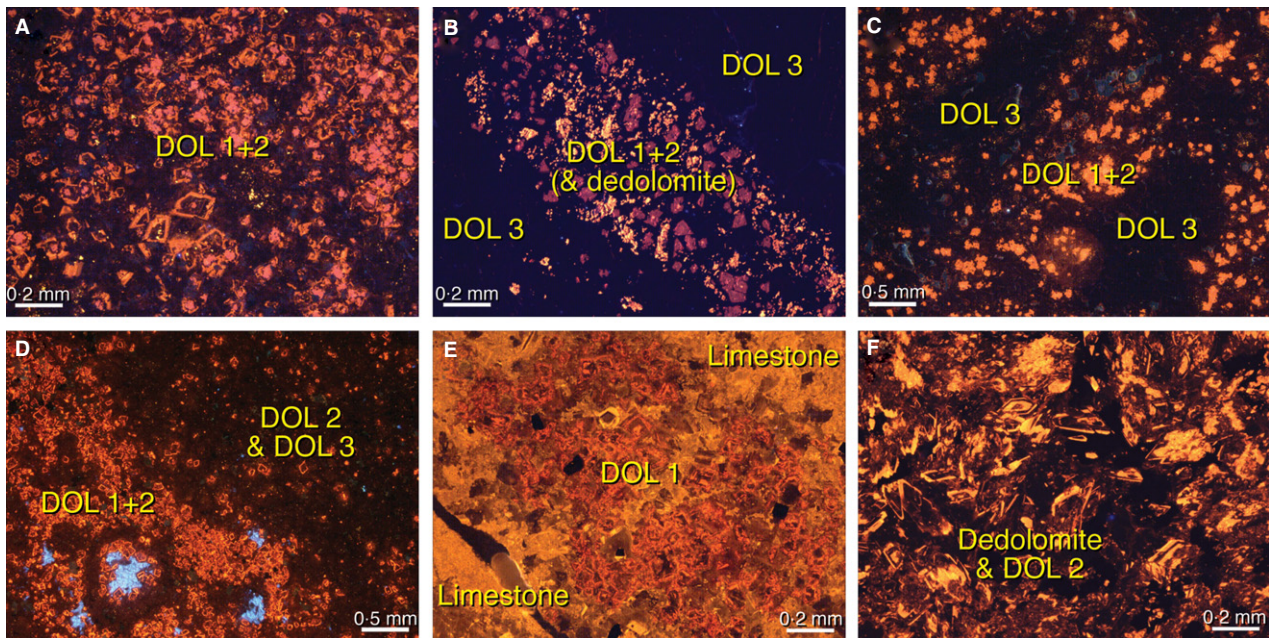
Fig. 10. CL photomicrographs of replacive and pore-filling dolomite. All have 0·2 mm scales [except for (C) and (D), 0·5 mm scales]. DOL 1 is red-CL, DOL 2 and DOL 3 are non-CL. (A) Zoned DOL 1, overgrown and partly replaced by DOL 2. Knockrushen Formation, Strand Hall. (B) DOL 1+2 with minor dedolomitization (bright yellow) cut by DOL 3 cemented veins. Bowland Shale Formation, Poyllvaaish. (C) Corroded DOL 1 overgrown by DOL 2 and DOL 3, with DOL 3 cement in cross-cutting vein. Knockrushen Formation, near Scarlett Point. (D) Pack/grainstone with replacive DOL 1+2 (bottom left) and DOL 2+3 (top right), bright blue is late diagenetic void-filling dickite. Derbyhaven Formation, Turkeyland Quarry. (E) Silty lime pack/grainstone showing partial replacement by zoned DOL 1. Derbyhaven Formation, Cass-ny-Hawin. (F) Severely dedolomitized sample, DOL 1+2 have been mostly replaced by Fe-oxide (black) and non-ferroan calcite (bright-non-CL zoned). Balladoole Formation, close to Balladoole mineral deposit.

crystal terminations that extend into open space and that can show one or more, thin, dull red to dull brown bands (Fig. 11A to F). Bright yellow-orange speckles or mottles are present where crystals have undergone dedolomitization (for example, Fig. 11E and F). More evidence of compositional zoning in DOL 3 is revealed by BSEM than by CL (Fig. 11G to I), with multiple concentric zones and some sectoral zones being revealed by relative variations in Mg^{2+}/Fe^{2+} ratio (confirmed by energy dispersive X-ray analysis). These are not seen in CL because of the quenching effect of the high iron content. Detailed concentric zoning patterns revealed by BSEM are not correlatable between geobodies, but a bipartite division into generally darker poorly zoned DOL 3a and brighter zoned DOL 3b is possible in many cases (Fig. 11G to I). At Derbyhaven and Balladoole, the interface between these shows at least one fracturing (and minor corrosion) event, and close to the Derbyhaven to Cass-ny-Hawin north-east/south-west fault, DOL 3a is mantled

by hematite (Fig. 12B). Saddle ankerite equivalent to DOL 3 in the Bowland Shale veins at Poyllvaaish is non-CL and unzoned in BSEM, despite subtle staining variations that suggest more than one episode of dilation and fill. Subsequent milky calcite in the veins is bright orange in CL and unzoned.

Bright and dark mottling in BSEM images of DOL 3 corresponds to Fe-oxide and calcite produced during dedolomitization, and this calcite locally overgrows the dolomite as cement. The calcite is either bright yellow-orange CL, or non-CL with multiple bright zones (Fig. 11B, C and E). Similar CL patterns occur in the late stage limpid calcite of the Bowland Shale veins (for example, Fig. 8C).

The sphalerite-rich breccia deposit at Balladoole contains the same three dolomite stages described above. Breccia clasts are replaced by minor DOL 1 and pervasive DOL 2, and the saddle dolomite cement between them and lining vugs corresponds to DOL 3. Both DOL 2 and DOL 3 post-date several fracturing episodes,
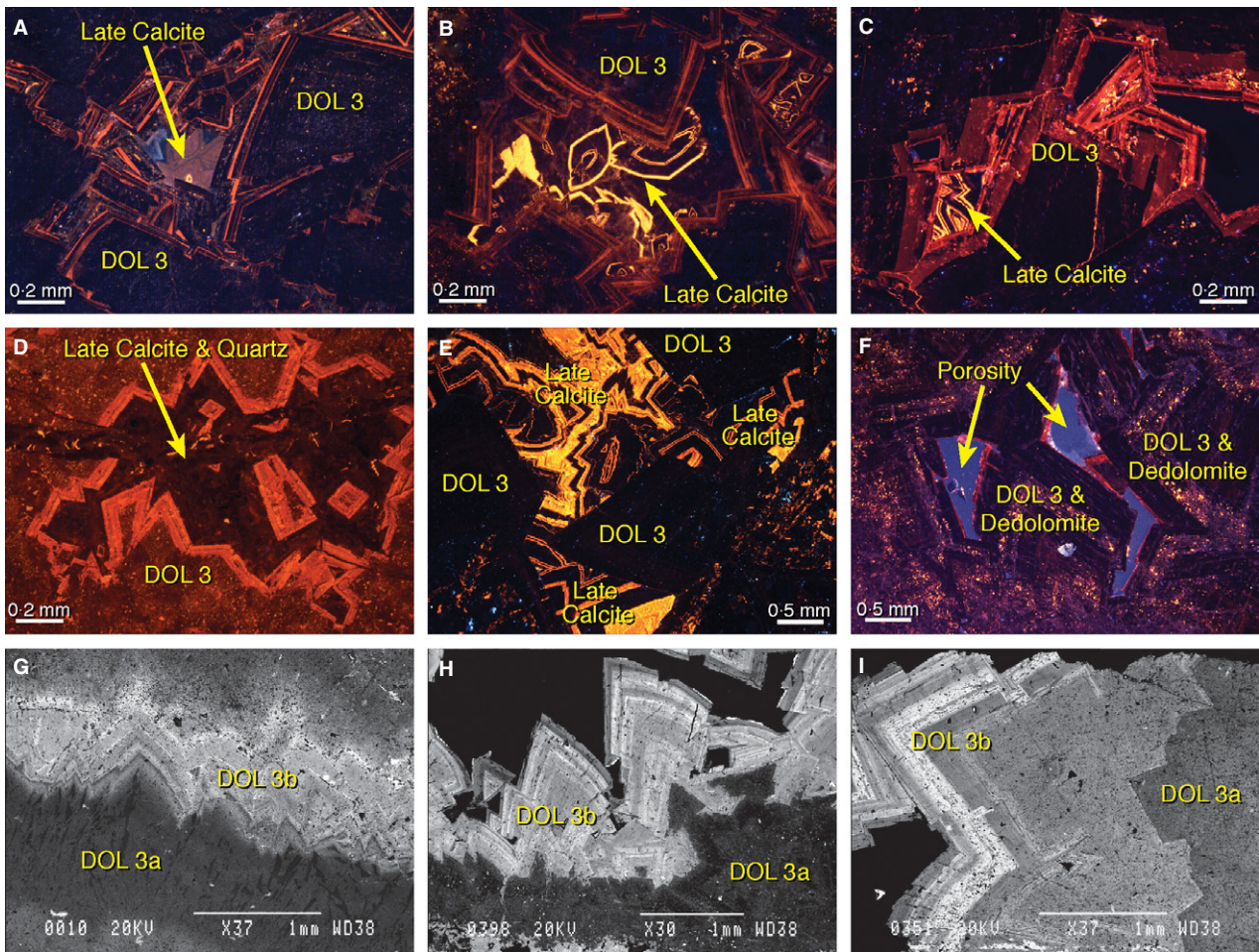
Fig. 11. Photomicrographs of variable zoning in DOL 3 and late calcite cements; see text for discussion. (A) to (F) are in CL and (A) to (D) have 0·2 mm scales, (E) and (F) have 0. 5 mm scales; (G) to (I) are in BSEM and have 1 mm scales. (A) Balladoole Formation, near Balladoole fault. (B) Balladoole Formation, within Balladoole mineral deposit. (C) Balladoole Formation, Cross Welkin Hill Quarry. (D) Bowland Shale Formation, Scarlett Point. (E) Derbyhaven Formation, Derbyhaven. (F) Derbyhaven Formation, Turkeyland Quarry. (G) Balladoole Formation, within Balladoole mineral deposit. (H) Bowland Shale Formation, Scarlett Point. (I) Derbyhaven Formation, Derbyhaven.

non-CL and blue CL stages of quartz, and most of the metal sulphides; they also pre-date a final brown-CL quartz precipitate (Shelton *et al.*, 2011).

Figure 13 presents a composite paragenesis for the dolomite geobodies, drawing on the observations of this study and integrating them with results from the Balladoole mineral deposit (Shelton *et al.*, 2011) and observations of Dickson & Coleman (1980). The paragenesis also includes thin veins of dull CL calcite that locally post-date the dolomitization, and dark blue CL dickite that is a minor late stage precipitate specific to the Derbyhaven area (Fig. 10D; also see Maliva *et al.*, 1999).

Fluid inclusions

Fluid inclusion microthermometry was carried out on DOL 3 and a small number of DOL 2 samples from across the study area, as well as ankerite (= DOL 3) and calcite samples from Bowland Shale veins. Results were integrated with those from the Balladoole sphalerite breccia deposit and Zn–Pb–Cu vein mineralization hosted by Manx Group metasedimentary rocks at Bradda Head (Shelton *et al.*, 2011). There is a broad spread of results, but several underlying patterns are apparent (Fig. 14, Table S2). Dolomite T_h values range from 58 to 292°C and salinities calculated from final ice melting (T_m)
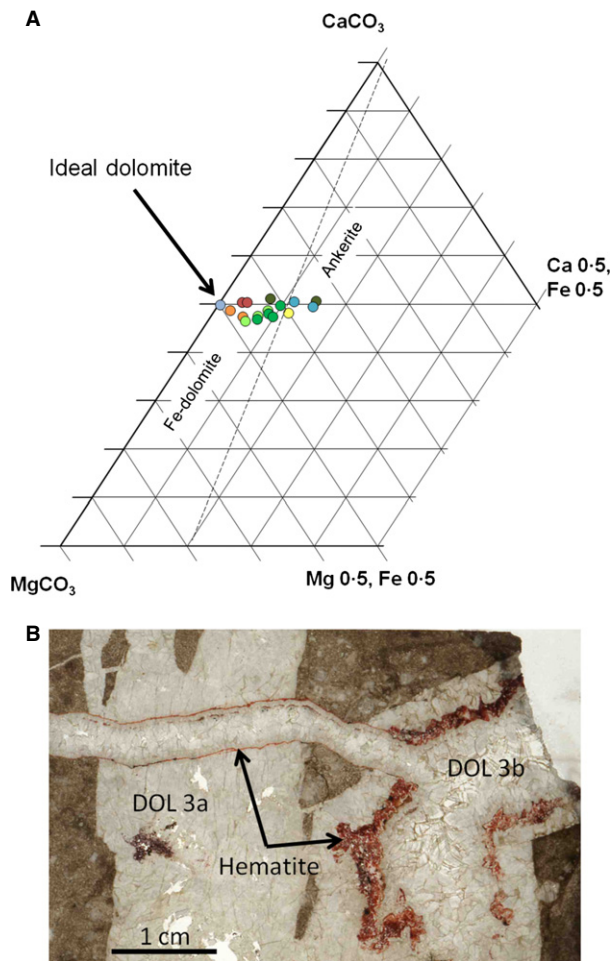
A

B

Fig. 12. (A) Major element chemistry of DOL 3 cement. Colours refer to different sampling locations (see Fig. S3). No geographical or stratigraphic trends in composition are evident. (B) Hematite intergrown between DOL 3a and DOL 3b from Derbyhaven.

temperatures range from 6·8 to 24·8 wt% NaCl equivalent. However, frequent eutectic temperatures below −22·5°C suggest complex brines probably containing additional solutes such as $CaCl_2$ (Zhang & Frantz, 1989).

The data show that a majority of values cluster between 80 to 130°C and 19 to 25 wt% NaCl equivalent, with two trends towards higher T_h and towards lower salinity, respectively (Fig. 14A). Dolomite samples on these trends have no consistent stratigraphic relationship; nor do they display any geographical trend, suggesting that parent fluid compositions and temperatures varied both temporally and spatially. However, ankerite veins from the Bowland Shale at Poyllvaaish all plot on the high T_h trend, and the highest temperature DOL 3 values are from locations close to major faults (Balladoole and Turkeyland). The main data cluster also coincides with fluid inclusions from sphalerite and much of the stage III quartz which pre-dates DOL 2 and DOL 3 in the Balladoole sphalerite breccia deposit, as well as late stage calcite veins in undolomitized limestones (Fig. 14B).

Inclusions in stage I quartz pods at Balladoole fall into two groups. The first group (stage 1a) has much higher T_h values (318 to 445°C) than the dolomites but similar elevated salinities (20 to 23 wt% NaCl eq.). The second group (stage 1b) has similar T_h values (271 to 467°C) but even higher salinities (36 to 46 wt% NaCl eq.) and contains halite daughter crystals (Fig. 14B). The latter were attributed by Shelton *et al.* (2011) to possible boiling of a lower salinity fluid at relatively shallow burial. Inclusions
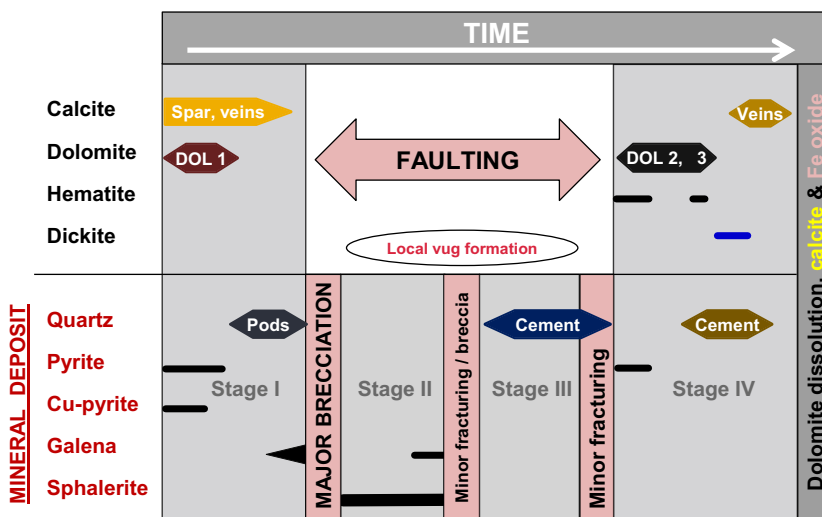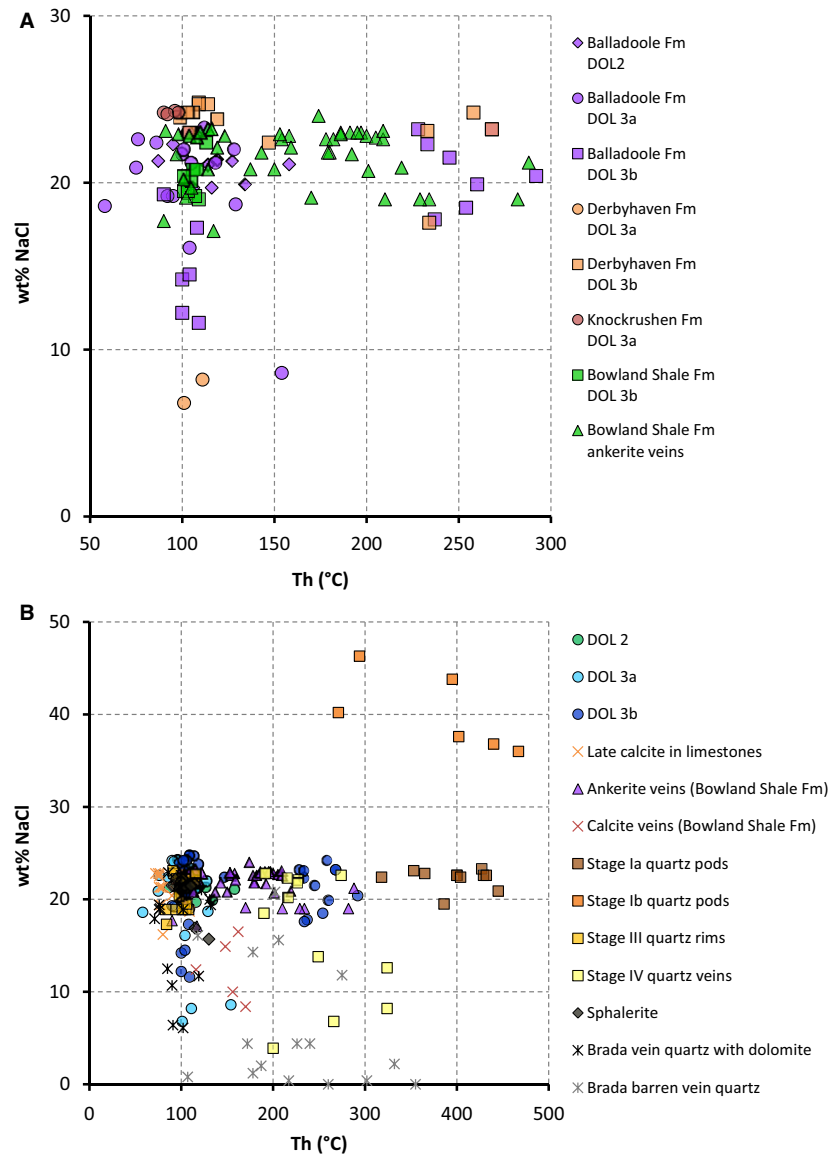

Fig. 13. Composite paragenetic history for the dolomite geobodies, including the Balladoole Zn deposit. Quartz and dolomite stages can be discriminated by CL, as represented by the colours on the figure. Early limestone diagenesis is dominated by early non-ferroan bladed to equant sparry calcite and subsequent coarse, ferroan sparry calcite.

Fig. 14. (A) T_h versus salinity data for fluid inclusions in DOL 2, DOL 3a and DOL 3b. (B) Additional T_h versus salinity data from fluid inclusions in calcite veins, plus data from Shelton *et al.* (2011) from Balladoole Zn deposit and quartz-dolomite veins in the Manx Group at Bradda Head. Note the different scale on the *x*-axis. In Fig. S1A groups the fluid inclusion results with respect to geographical sampling location.

from vein quartz with dolomite from the Manx Group at Bradda Head overlie the salinity trend defined by the DOL 2 and DOL 3 data. Stage IV quartz veins from the Balladoole mineral deposit produce wide ranges of T_h and salinity values (190 to 324°C, 4 to 23 wt% NaCl eq.; Fig. 14B), overlapping those from barren quartz veins from Bradda Head (107 to 355°C; 0 to 21 wt% NaCl eq.) that also contain three-phase H_2O-CO_2 inclusions.

Stable isotopes

Carbon and oxygen isotope data are plotted in Fig. 15. It was not possible to physically isolate DOL 1 for analysis, and stable isotope data are grouped according to whether the samples were

mixtures of DOL 1 and DOL 2 ('DOL 1+2'), mostly DOL 2, or just DOL 3. Ankerite veins at Poyllvaaish are depicted separately, although they are assumed to be equivalent to DOL 3. Vein calcites and host limestones (bulk samples but drilled to avoid visible cements) are also plotted. The vast majority of dolomite and ankerite samples define a wide range in $\delta^{18}O$ (−5·1 to −16·0‰ VPDB) and a narrower range in $\delta^{13}C$ values (−3·1 to +3·6‰ VPDB). There is considerable overlap among the different dolomite types, although the lowest dolomite $\delta^{18}O$ values are for DOL 3b and ankerite cements and the highest values are dominated by DOL 1+2 samples. Dolomite 3 cements define a crude positive correlation, whereas ankerite samples plot with marked negative covariance (actually two paral-
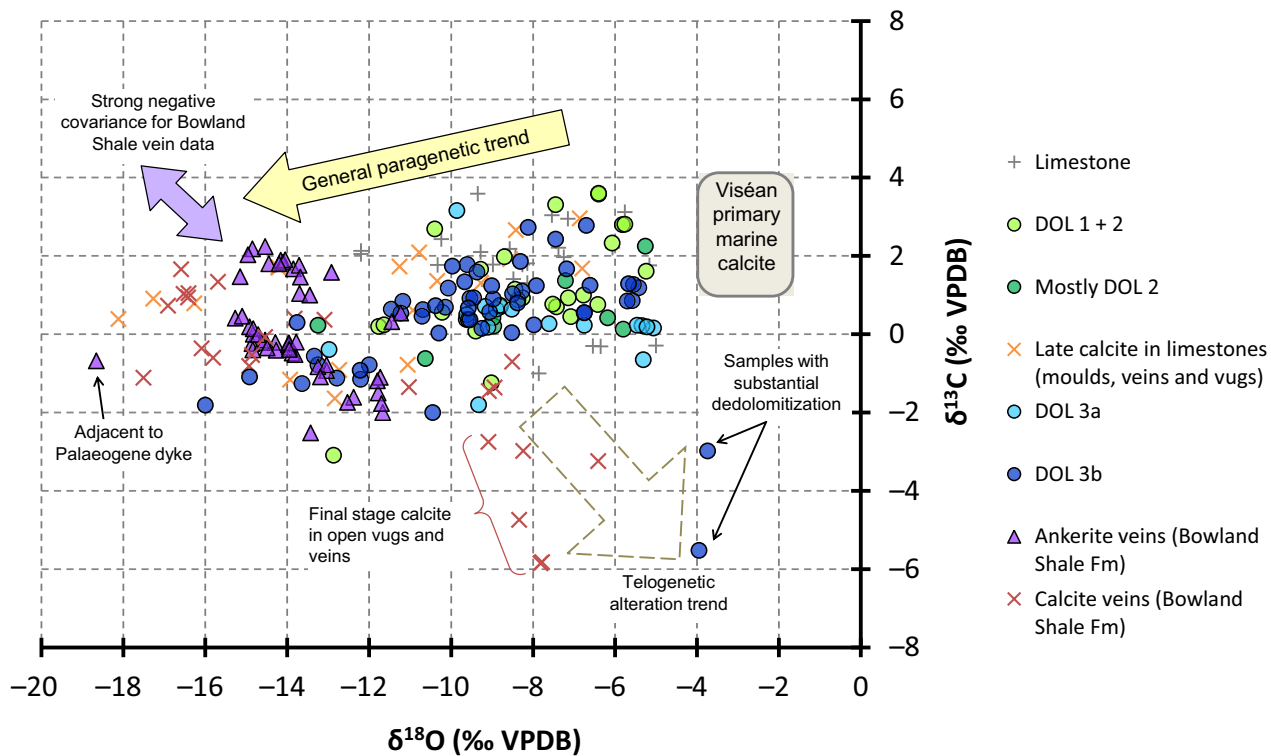
Fig. 15. $\delta^{13}C$ and $\delta^{18}O$ data for dolomite, ankerite and calcite. See text for discussion of annotated trends. Barring two dedolomitized samples, pooled DOL 3 data define a crude positive covariance ($R^2 = 0.49$). Ankerite samples from Poyllvaaish define two parallel negative covariant trends; the upper is from narrow (<2 cm) veins in the 'Black Marble Quarry' and the lower is from thicker veins (2 to 10 cm) on the foreshore ≤25 m away. Corresponding R^2 values are 0.52 and 0.61, respectively. The ankerite with the lowest $\delta^{18}O$ value was collected close to a Palaeogene dyke and has been thermally altered. In the supplementary data, Fig. S1B groups the stable isotope results with respect to geographical sampling location, and Fig. S1C compares them to those of Dickson & Coleman (1980).

lel trends, which correspond to veins from the foreshore exposure and the adjacent quarry, respectively. Multiple samples across selected DOL 3 and ankerite veins show progressive decreases in $\delta^{18}O$ values, by as much as 4·5‰ (Fig. 15). There is no consistent stratigraphic or geographical pattern within the DOL 3 data (Fig. S1B), and the two outlying samples with low $\delta^{13}C$ (−3·0 and −5·5‰ VPDB) but relatively high $\delta^{18}O$ (−3·7 and −4·0‰ VPDB) values displayed significant dedolomitization (Fig. 15).

Late calcite veins in undolomitized limestone define a broad envelope in O–C isotope space that is approximately the same as that for the dolomites, albeit displaced roughly 2‰ towards lower $\delta^{18}O$ values. Bowland Shale-hosted vein calcites from Poyllvaaish fall into two subsets; coarse milky white calcites have low $\delta^{18}O$ values (−11·0 to −17·5‰ VPDB) and unremarkable $\delta^{13}C$ values (+0·9 to −1·4‰ VPDB), whereas the limpid calcites in the cen-

tre of some veins have higher $\delta^{18}O$ values (−6·4 to −8·3‰ VPDB) but lower $\delta^{13}C$ values (−0·7 to −5·9‰ VPDB).

Stable isotope data were collected from the Derbyhaven Formation by Dickson & Coleman (1980). Their results for late stage ferroan calcite and dolomite fall within the corresponding data fields in Fig. 15, and confirm the general paragenetic trend towards lower $\delta^{18}O$ values. Early calcite cements, which were not sampled in the current study, had relatively high $\delta^{18}O$ values (−4·7 to −2·6‰ VPDB). These are higher than values for bulk limestones sampled by Dickson & Coleman (op. cit.) (−9·3 to −5·5‰ VPDB) and in the present study (−12·2 to −5·0‰ VPDB), suggesting that bulk limestones incorporate late diagenetic calcite at a scale below visual resolution.

Strontium isotopes ratios for replacive dolomite (DOL 2 and DOL 1+2), DOL 3 cement, and vein ankerites yield similar ranges, between
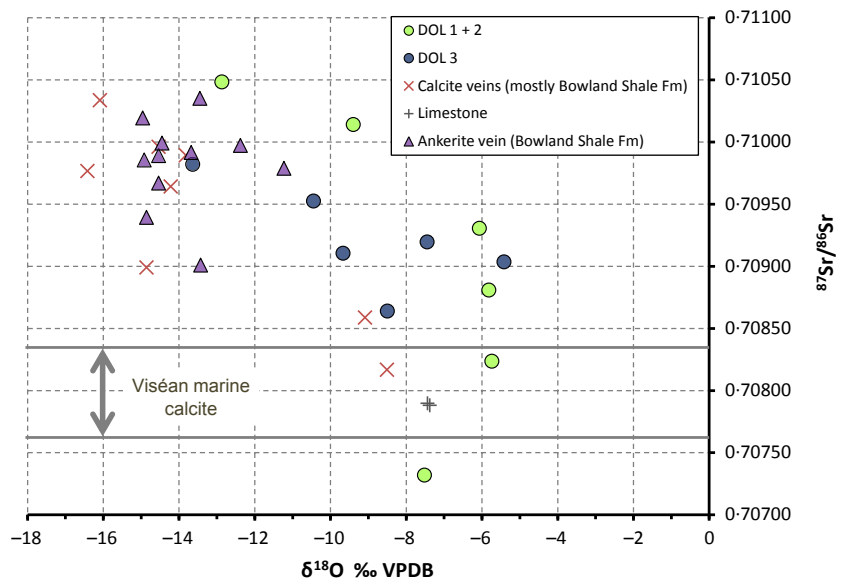
Fig 16. Strontium isotope ratios and corresponding δ¹⁸O values for dolomite, ankerite and vein calcite samples, compared to diagenetically unaltered Viséan marine calcites. The lack of a covariant trend reflects precipitation during mixing of compositionally and thermally dissimilar fluids.

0·707320 and 0·710484 (Fig. 16). Calcite veins post-dating DOL 3/ankerite have values from 0·708168 to 0·710337. Two undolomitized limestone samples yielded $^{87}Sr/^{86}Sr$ ratios of 0·707882 and 0·707898, which fall within the range of Viséan sea water compositions based on analysis of well-preserved marine fossils (McArthur *et al.*, 2001). Taken as a whole, the data show a trend of increasing $^{87}Sr/^{86}Sr$ with decreasing $^{18}O/^{16}O$, but there is no paragenetic, geographical or stratigraphic pattern. Plotting strontium and carbon isotope values together produces no discernible trends.

Sulphur isotope ratios in sulphide minerals were not measured in this study. However, Shelton *et al.* (2011) reported δ³⁴S data obtained from samples collected from the Balladoole sphalerite mineralization. Values of +6·5 to +6·9‰ VCDT were essentially identical to examples of sphalerite-bearing ores hosted by Manx Group metasedimentary rocks across the Isle of Man (Crowley *et al.*, 1997a).

DISCUSSION

Origin and evolution of the dolomitizing fluids

Replacive dolomite and saddle dolomite cement that is associated spatially with faults and fractures in Mississippian limestones of the south-eastern Isle of Man provides a record of fluid–rock interaction and mass transport across formation boundaries. In particular, Mg^{2+} and

Fe^{2+} must have been imported into the limestones, there being no internal sources for these elements other than the Scarlett Volcanic Member, which can be discounted on isotopic evidence (discussed below). However, determining the origin of dolomitizing fluids is not trivial. Stable isotope, fluid inclusion and petrographic data encompass a wide range of values that probably reflect fluids of varying composition and temperature, which may have interacted with diverse rock types during transport. It is clear that, locally, DOL 2 and initial DOL 3 cement overlap in composition and reflect a common fluid parentage. Therefore, they can conveniently be considered together with the proviso that DOL 2 may retain more of a residual 'signature' of the precursor limestone as well as physically incorporating disseminated DOL 1 cores that (based on preservation of CL zoning) have not been fully recrystallized (Mazzullo, 1992). However, the lack of simple two-component mixing trends in stable isotope or T_h-salinity space shows that the dolomitizing fluids evolved spatially and temporally within the fault-fracture system as they interacted with host limestone and resident pore fluids.

Burial history

The burial history of the host limestones is impossible to reconstruct precisely, owing to the poorly constrained uplift history of the Manx region during Variscan compression, during the Late Jurassic–Early Cretaceous interval, and associated with Palaeogene uplift and erosion

(e.g. Cope, 1997; Newman, 1999; Holford *et al.*, 2005). There are also uncertainties surrounding past heat flow values, including the possibility of transient elevated geothermal gradients associated with Late Viséan volcanism, Early Mesozoic rifting in the East Irish Sea Basin and Palaeogene thermal doming (e.g. Chadwick *et al.*, 1994, 2001). Interpretations of regional vitrinite reflectance (R_0) data and apatite fission track (AFTA) data from the East Irish Sea and Peel basins yielded maximum palaeotemperatures of ≤120°C that were attained between the Late Carboniferous and Palaeogene (Green *et al.*, 1997; Newman, 1999). Green *et al.* (2012) have recently estimated 800 ± 300 m of post-Carboniferous exhumation on the Isle of Man and eastern margins of the East Irish Sea Basin, and peak palaeotemperatures of 50 to 110°C. Maximum burial depths and temperatures in offshore basins were unlikely to have been significantly higher (Chadwick *et al.*, 2001).

Racey *et al.* (1999) reported thermal maturity data from cored samples in shallow Carboniferous subcrop from the north of the Isle of Man, and from the Bowland Shale Formation outcrop at Poyllvaaish. Vitrinite reflectance mostly ranged from 0·5 to 1·0 for the former, but up to 2·3 for the latter. The lower values are consistent with Cretaceous peak burial temperatures of 105 to 115°C, modelled on AFTA data from the same location (Green *et al.*, 1997). The Poyllvaaish data are comparable to R_0 measurements collected by one of the authors (SFC) from several calcareous mudstones within the Derbyhaven, Knockrushen and Bowland Shale Formations and presented in Fig. S2. These data reveal a quasi-normal distribution with a dominant mode of 2·4 to 2·8, and a range of 2·1 to 3·1, suggesting maximum temperatures of *ca* 220 to 250°C for 'normal' burial diagenesis or 260 to 280°C for an elevated heat flow typical of geothermal systems (Sweeney & Burnham, 1990). Such high R_0 values are inconsistent with regional data and the long-lived structurally high context of the Manx–Lakeland Ridge. They are most likely to be related to localized and short-lived heating associated with eruption of the Scarlett Volcanic Member lavas, or to high-temperature fluid circulation as recorded in the dolomite bodies. In support of the latter, Racey *et al.* (1999) documented maximum temperatures fluctuating between 124°C and 185°C over *ca* 50 m of Namurian strata in the Ballavarkish borehole to the north of the island and far removed from the outcrop of the Scarlett Volcanic Member. Deeper

in the same borehole are faulted and vuggy 'sucrosic' dolomites of probable Viséan age (Quirk & Kimbell, 1997).

Origin of salinity

Fluid inclusion data in Fig. 14 provide the most direct evidence for the nature and origin of the dolomitizing fluids. The two intersecting trends suggest mixing and cooling of hydrothermal (≤292°C) hypersaline (≤25 wt% NaCl eq.) allochthonous fluids with resident pore fluids in the limestones. It is significant that inclusions in sphalerite and associated quartz from the Balladoole mineral deposit plot with the main cluster of DOL 3 and vein calcite data. This coincidence suggests a genetic link to mineralization in the Manx Group basement strata and so implies that at least one of the key fluids was transmitted up into the overlying limestones (Shelton *et al.*, 2011). However, the basement metasedimentary rocks were deposited in a distal submarine fan setting and contain no evaporites (Woodcock & Barnes, 1999). Moreover, the high fluid-inclusion salinities are impossible to attain from silicate–brine interactions. Values of >16 to 17 wt% NaCl imply involvement of sea water evaporated beyond gypsum saturation, and although maximum values (24·8 wt% NaCl eq.) are slightly less than halite saturation (*ca* 26·3 wt% NaCl eq.) these may have been diluted by mixing with resident pore fluids. Therefore, highly evaporated sea water is implicated, possibly augmented by halite dissolution, as has been deduced for other examples of fault-fracture-related dolomite and carbonate-hosted base metal deposits (e.g. Lonnee & Machel, 2006; Conliffe *et al.*, 2010; Gregg & Shelton, 2012).

There are no evaporites or peritidal facies preserved in the limestones on the Isle of Man, and deepening in the Late Viséan (Fig. 2) suggests that they are unlikely to have been present but later eroded. Viséan anhydrites are present in the Solway Basin north-east of the Isle of Man (Ward, 1997) and have been linked isotopically to barite mineralization in Carboniferous limestones of the North Pennines ore field (Crowley *et al.*, 1997b). Similar evaporites may have been located in parts of the East Irish Sea and Peel Basins (Chadwick *et al.*, 2001). More extensive but halokinetically disrupted salt deposits of Late Permian and Early Triassic age reach up to 250 m thickness in parts of the East Irish Sea Basin including the

Eubonia sub-basin to the south-east of the Manx–Lakeland Ridge (Fig. 1A). Tens to hundreds of metres thick evaporite deposits are also present in the Late Triassic Mercia Mudstone Group, which was deposited across most of the north-western East Irish Sea and Peel Basins (Cowan *et al.*, 1999). There is no evidence for the former presence of these evaporites over the Isle of Man, but they may have been the source of hypersaline fluids that migrated from offshore basins. It is postulated that post-evaporite brines can migrate from tens to more than 100 km to become involved in fault-related dolomitization (e.g. Lonnee & Machel, 2006; Wendte *et al.*, 2009).

Evidence for hydrothermal fluid–rock interactions

The presence of hematite and dickite broadly coeval with DOL 3 precipitation at Derbyhaven may be related to fluid–rock interaction in the metasedimentary basement (for example, the Manx Group at Cass-ny-Hawin is iron-enriched) or in Permo-Triassic red beds formerly overlying the Viséan limestones and/or offshore. Ferrous iron cannot be transported in fluids bearing significant sulphide or bicarbonate, and dickite precipitation in carbonates is evidence of enhanced aluminium mobility potentially catalysed by organic acid anions (Maliva *et al.*, 1999). The latter may also have been involved in iron reduction, and so hematite and dickite could be subtle indicators of incipient hydrocarbon maturation and fluid expulsion from offshore basins coinciding with the waning of the hydrothermal fluid circulation system. Bitumen inclusions in late stage calcite associated with dickite were reported by Maliva *et al.* (1999), and Parnell (1997) reported bitumen intergrown with high-temperature quartz in calcitic veins at Castletown and Poyllvaaish (T_h of 200 to 220°C, similar to stage IV at Balladoole). However, no bitumen has been observed in the current study and 'apparent' bitumen was always found to be mixtures of clay and Fe-oxide. Once mobilized, Al would have remained soluble in hydrothermal fluids of low pH (e.g. Rusk *et al.*, 2008). Reaction of low-pH Fe-bearing, Al-bearing and Si-bearing hydrothermal fluids with the host limestones was probably sufficient to cause the localized kaolinite and hematite precipitation.

Interaction of hydrothermal fluids with crustal silicates is also evidenced by the Sr isotope data (Fig. 16). Most of the DOL 3 values are more radiogenic than Phanerozoic sea water (McArthur *et al.*, 2000) and probably gained ^{87}Sr from dissolution of feldspars or micas in basement fracture systems or siliciclastic aquifers. Significantly, these data argue against fluid interaction with Scarlett Member submarine volcanic rocks, which are basaltic in composition and probably had lower Sr isotope ratios than coeval sea water. The general relation of increased ^{87}Sr/^{86}Sr and lower δ^{18}O values (Fig. 16), but with a lack of geographical or paragenetic trends, indicates that allochthonous fluids from different fault-fracture conduits achieved varying degrees of equilibration with host limestones and their resident fluids. Returning to the fluid-inclusion data in Fig. 14, these resident fluids may account for the trend away from the main data cluster towards lower salinities, but given that Manx Group vein samples also fall on this trend, it could also represent a separate allochthonous fluid that was entrained from the basement into the hydrothermal flow cells. If so, data from the stage IV quartz at Balladoole suggest that its contribution may have increased with time. Involvement of two major allochthonous fluids (hydrothermal–hypersaline and mesothermal–mesosaline) could explain the 'inverted L' pattern of dolomite data on Fig. 14.

Stable isotopes

Carbon and oxygen isotopes provide additional constraints upon the nature of the dolomitizing fluids. Pristine brachiopods and marine cements from European Viséan limestones have δ^{18}O and δ^{13}C values of -1.5 to $-4\%_0$ VPDB and $+1$ to $+4\%_0$ VPDB, respectively (Bruckschen *et al.*, 1999; Prokoph *et al.*, 2008; Grossman, 2012). Assuming equilibrium isotopic fractionation, the carbonate δ^{18}O values correspond to sea water δ^{18}O values of -0.2 to $-2.8\%_0$ VSMOW at a depositional temperature of 20°C. There is no evidence of palaeokarst or syn-depositional emergence fabrics in the succession, so it is reasonable to assume that the resident pore fluids in the limestones throughout early diagenesis were of marine parentage.

Combined isotopic and fluid-inclusion data are only available for a small number of samples, and although the highest T_h samples are among the most ^{18}O-depleted, there is no consistent relation (Fig. 17). This fact supports the interpretation of precipitation during mixing of compositionally and thermally dissimilar fluids. The wide range in DOL 3 and ankerite δ^{18}O values includes some compositional zoning, but clearly also requires variations in fluid composi-
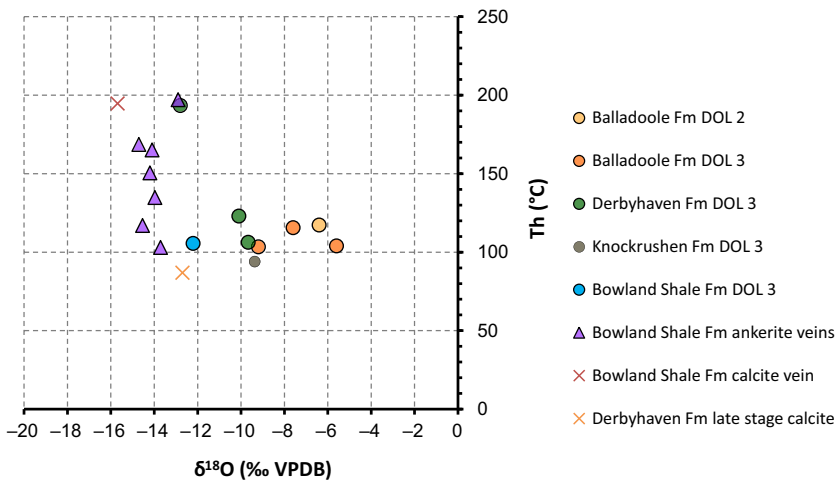
Fig. 17. Cross-plot of $\delta^{18}O$ values versus fluid-inclusion homogenization temperature for samples for which both parameters were measured.

tion and/or temperature between different fault-fracture-related geobodies.

Equilibrium oxygen isotope fractionation curves for data from carbonates (this study), quartz from the Balladoole mineral deposit (Shelton *et al.*, 2011) and dickite from the Derbyhaven Formation (Dickson & Coleman, 1980), in combination with T_h ranges, allow fluid oxygen isotope compositions ($\delta^{18}O_{water}$ values) to be estimated (Fig. 18). In the absence of fluid ionic compositions, the influence of hypersalinity on isotope fractionation has not been incorporated, although it should not be a major factor at the temperatures being considered (Horita, 2005).

Stage III quartz ($\delta^{18}O$ of +18·3‰ VSMOW) precipitated from waters with $\delta^{18}O$ values of −5·1 to −0·8‰ VSMOW, close to the value of original marine pore water. The majority of analysed DOL 3 samples precipitated from evolved waters with $\delta^{18}O$ values of +2·2 to +7·5‰ VSMOW, and stage IV quartz ($\delta^{18}O$ of +19·8‰ VSMOW) precipitated from highly evolved waters with $\delta^{18}O$ values of +6·4 to +13·2‰ VSMOW. The progressive increase in $\delta^{18}O_{water}$ values may be explained in several ways. It is a likely consequence of water–rock interaction as hydrothermal fluids circulated through basement and/or offshore sedimentary basin strata; it may also reflect incorporation into the palaeohydrological system of the residual pore fluids in evaporite units that contributed the high salinities. Alternatively, the shift could represent increasing equilibration of waters with host carbonate at higher temperatures and lower water:rock ratios. Similar ^{18}O enrichment is characteristic of many other examples of hydrothermal dolomitization and carbonate-hosted base metal mineralization where isotopic and fluid-inclusion data have

been collected (e.g. Wright *et al.*, 2000, 2004; Johnson *et al.*, 2009).

The wide range in $\delta^{18}O_{water}$ compositions calculated for DOL 2 and DOL 3 conforms to their spread of precipitation temperatures and salinities (Fig. 14A). It is a consequence of the allochthonous fluids interacting with host strata and mixing with resident evolved Viséan marine pore fluids as they cooled and permeated the limestones adjacent to fault-fracture conduits. Carbon isotope values that are clustered around $\delta^{13}C = 0‰$ VPDB suggest that the dissolved carbon reservoir was dominated by exchange with the host limestones. A subtle paragenetic trend to slightly lower values might indicate minor organogenic carbon incorporation from the petroliferous offshore basins. In contrast, $\delta^{18}O_{water}$ values were much less buffered by the host limestones. At the temperatures of DOL 2 to DOL 3, precipitation waters in equilibrium with the host limestone would have $\delta^{18}O$ values between +6·7‰ and +23·5‰ VSMOW (Fig. 18). The lowest degree of water–rock equilibration (lowest $\delta^{18}O_{carbonate}$ values) is unsurprisingly displayed by vein-hosted ankerites in the argillaceous Bowland Shale Formation. A similar degree of disequilibrium is apparent for the fluids that precipitated stage III and IV quartz in the Balladoole sphalerite deposit. In contrast, dolomites within host limestones formed after more water–rock interaction, as evidenced by higher $\delta^{18}O_{carbonate}$ values and generally lower $^{87}Sr/^{86}Sr$ ratios (Fig. 15). Some relatively ^{18}O-enriched DOL 2 samples also contain a contribution from residual DOL 1.

The lack of isotopic data for pure DOL 1 complicates its interpretation. Nevertheless, based on the paragenetic trends it is likely that DOL 1
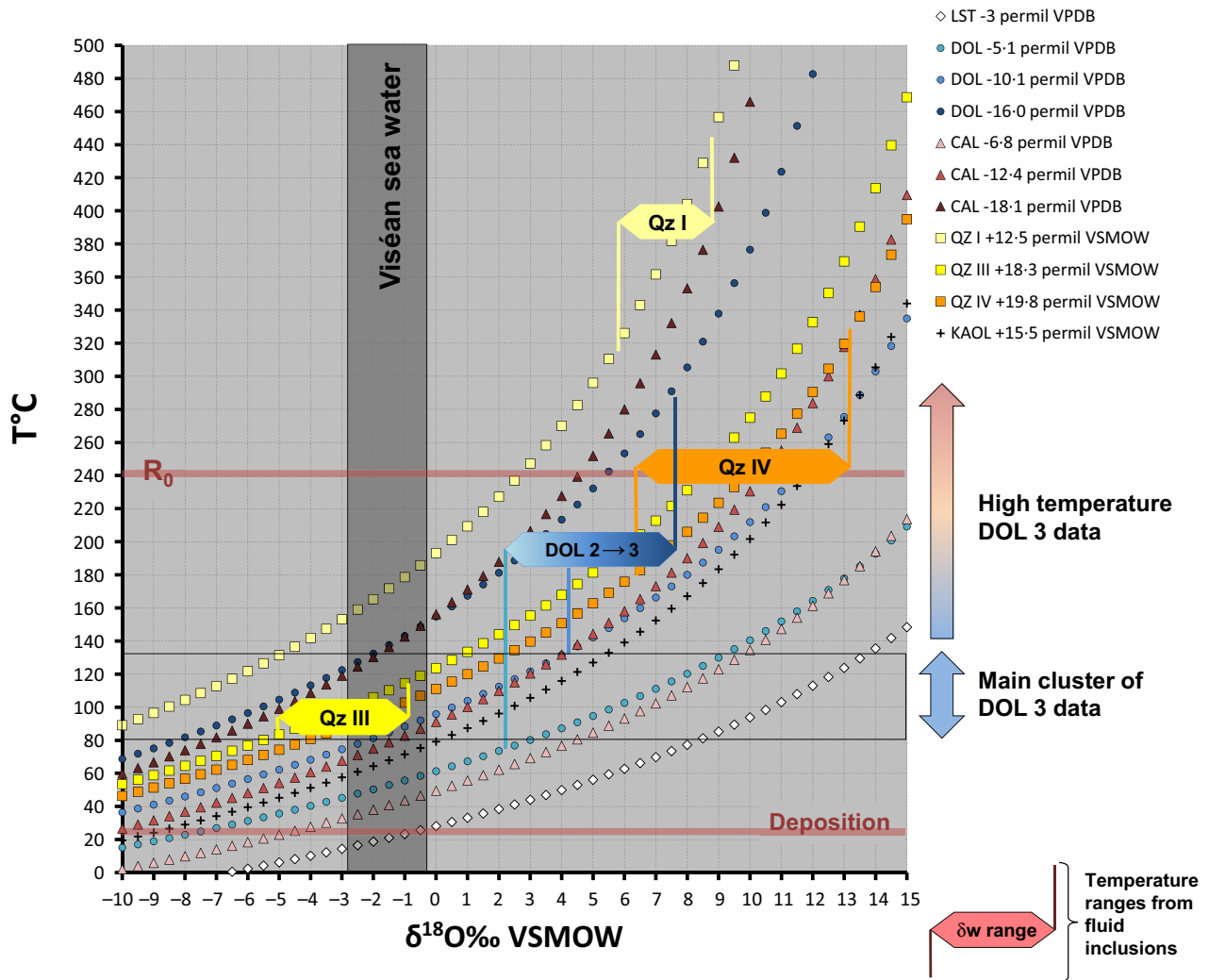
Fig. 18. Equilibrium oxygen isotope fractionation plot for selected dolomite and calcite compositions, plus quartz cements from the Balladoole Zn deposit and dickite from the Derbyhaven Formation. Narrow vertical bars indicate T_h ranges for different precipitates and broad horizontal bars indicate corresponding δw ($\delta^{18}O_{water}$) values. Equations used take the form of $10^3 \ln\alpha = (A \times 10^6 \times T^{-2}) + B$, where A and B are 2·78 and −2·89 for calcite (Friedman & O'Neil, 1977), 3·23 and −3·29 for dolomite (Sheppard & Schwarcz, 1970), 3·306 and −2·71 for quartz (Zhang *et al.*, 1989), and 2·76 and −6·75 for kaolinite/dickite (Sheppard & Gilg, 1996). See text for discussion.

$\delta^{18}O$ values are higher than DOL 2 or DOL 3, and may therefore be more positive than *ca* −4‰ VPDB. As such, they would overlap or be more positive than the range for Viséan primary marine calcites. Taking into account a 3 ± 1‰ fractionation between co-genetic calcite and dolomite at 25°C (Land, 1980), DOL 1 could reasonably have formed at shallow burial from original marine or slightly evolved pore fluids.

Stage I quartz represents an atypical case. It pre-dates all of the other fault-fracture-related precipitates in the Balladoole mineral deposit and mostly occurs in discontinuous pods that

may be veins that were dismembered by faulting and brecciation (Shelton *et al.*, 2011). Fluid inclusion salinities suggest that the quartz could represent the earliest stage of hydrothermal activity, but the very high temperatures may be more compatible with preceding events possibly associated with the eruption of the Scarlett Volcanics. Fluid compositions based on its $\delta^{18}O$ value of +12·5‰ VSMOW and temperature range of 318 to 445°C yield $\delta^{18}O_{water}$ values of +5·7 to +8·8‰ VSMOW.

Although fault-fracture-related dolomitization took place under the influence of hypersaline

and hydrothermal fluids, these were probably not responsible for the localized dedolomitization and latest stage calcite precipitation. A clear trend towards lower $\delta^{13}C$ and higher $\delta^{18}O$ values is associated with these samples (Fig. 15). The association of Fe-oxide with non-ferroan calcite, typically showing non-CL or bright CL and complex zoning (Figs 10F, 11B, 11C and 11E) suggests precipitation in relatively oxygenated near-surface fluids during uplift (cf. Milodowski *et al.*, 1998, stage 'ME9'). Assuming precipitation at 20°C, water in equilibrium with the highest values of these calcites ($\delta^{18}O = -6.4‰$ VPDB) would have had a $\delta^{18}O_{water}$ value of $-5.2‰$ VSMOW. By comparison, $\delta^{18}O$ values of modern spring and well waters in the Irish Sea region average between $-5‰$ and $-7‰$ VSMOW (http://www.bgs.ac.uk/nigl/SBA_Maps.htm, retrieved October 2012).

Source of magnesium

The source of magnesium for dolomitization is equivocal, and the data set does not lend itself to meaningful mass balance calculations. While some Mg^{2+} may have been released by fluid–rock interactions in the basement or clay mineral diagenesis in offshore basins, it is probable that the hydrothermal fluids were ultimately derived from sea water (Shelton *et al.*, 2011). Alternative magnesium sources sometimes considered in the hydrothermal dolomite literature include mafic or ultramafic igneous rocks (e.g. Lavoie & Chi, 2010). The Isle of Man is within a few tens of kilometres of the Iapetus Suture (Chadwick *et al.*, 2001). Ophiolites are known from south-west Scotland and Ireland but none are recorded within the known local geology. Moreover, major fluid interaction with the Scarlett volcanics has already been discounted based on Sr isotopes, and the same argument can be applied to any potential ultramafic bodies. Magnesium is, therefore, most likely to have been transported from the offshore basins in the hypersaline fluids that are recorded in the DOL 2 and DOL 3 fluid inclusions.

In summary, combined petrographic, fluid inclusion and isotopic evidence point to the interaction of (at least) three fluid end-members during hydrothermal fault-fracture-related dolomitization: (i) an allochthonous hypersaline fluid; (ii) an allochthonous moderate salinity fluid; and (iii) resident pore waters buried with the sedimentary rocks. Both allochthonous fluids passed through Manx Group basement, but the hypersaline fluid must either have originated as post-evaporite brines or have dissolved evaporites in offshore or (formerly) overlying strata. The latter is less attractive in terms of a potential Mg^{2+} source. Dolomitization and dolomite cementation took place at temperatures of *ca* 80 to 300°C as fluids cooled and infiltrated the limestones. The fact that a majority of samples give temperatures of *ca* 80 to 120°C suggests that cooling was an important kinetic drive for the dolomitization reaction, especially if the incoming fluids were initially calcite-saturated. All of the dolomitizing fluids were enriched in Fe^{2+} and Mg^{2+}, but only those tapped by certain faults and fractures had the chemistry and temperature history appropriate for precipitation of sphalerite, galena, quartz or hematite.

Timing of dolomitization and associated mineralization

Several lines of indirect and circumstantial evidence may be combined to evaluate the most likely timing of hydrothermal activity and dolomitization, although none are conclusive (Table 1). Essential requirements are a tectonic context suitable for large-scale fault-fracture hosted flow, a heat source, availability of evaporitic strata as a likely source of high salinity and Mg-rich residual brines, fluid access to the metasedimentary basement and a stress regime which favoured transmission along the most important north-east/south-west fault orientations. It is widely recognized that extensional or (especially) transtensional faulting is commonly associated with hydrothermal dolomitization (e.g. Davies & Smith, 2006; López-Horgue *et al.*, 2010). In some cases, the extension is within the context of a wider compressive regime, such as migration of a peripheral bulge during early stages of foreland basin development (Lavoie & Chi, 2010) or thrust-tip anticline development (Sharp *et al.*, 2010). In other cases hydrothermal or mesothermal dolomitization has been related to thrust tectonics, with fluids being expelled by tectonic loading of footwall basins – the so-called 'squeegee' model (Oliver, 1986; Ronchi *et al.*, 2012). However, it is difficult to reconcile such cases with elevated heat flow or the ability to circulate large volumes of fluid for prolonged time intervals (Machel, 2004).

Figure 4B and D shows that extensional–transtensional stress regimes would have favoured opening of reactivated Caledonian north-east/south-west faults in the Early Carboniferous (during and shortly after deposition of the

Table 1. Key evidence used in evaluating the most likely timing for hydrothermal fluid flow and dolomitization of the Viséan limestones on the Isle of Man.

Age	Stress field on key NNE to NE fault trends	Availability of highly evolved sea water or evaporite deposits	Potential for thermal anomaly	Dating evidence
Late Viséan	Extensional	Possible offshore or former onshore Early Viséan $CaSO_4$ (Solway Basin contains *ca* 100 m anhydrite)	Scarlett Volcanics Mb magmatism related to rift tectonics	Volcanics are close to $ZnS–SiO_2$ deposit, but not spatially related to other dolomites
Variscan (Late Carboniferous to Early Permian)	Compressional	No local evidence for this time interval	Offshore basins record evidence for deep (up to 4 km) burial in Late Carboniferous. Uplift-related cooling probably during inversion	Best for basement/off-shore basin dewatering? Fits Pb isotope model ages from basement Zn–Pb mineralization (310–280 Ma)
Triassic–Jurassic	Transtensional	Permian salts in offshore Eubonia and Peel basins, but not recorded onshore	Possible rift-related heating in Late Permian and Early Triassic	Palaeomagnetic dating of hematite within DOL 3 at Derbyhaven (245–230 Ma). Fits Pb isotope model ages from basement Zn–Pb mineralization (210–190 Ma). AFTA evidence for pre-Mid Jurassic thermal episode in central Ireland, active rifting in offshore basins
Palaeogene	Minor compression associated with thermal doming	Permian and Triassic salts buried in offshore basins	Regional elevated heat flow related to North Atlantic LIP	Circumstantial (AFTA, VR) evidence for hydrothermal activity in East Irish Sea Basin BUT dolomite bodies are not associated with dykes, and adjacent ankerite veins are metamorphosed by them

Viséan limestones) and again in the Permo-Triassic when the main phase of rifting took place in the East Irish Sea and Peel basins. In contrast, these faults would have been more likely to be sealed during the Late Carboniferous Variscan orogeny and in the Neogene. Although Variscan compression may have favoured dewatering of deeply buried offshore Carboniferous sedimentary successions, R_0 and AFTA data suggest regional cooling related to uplift rather than increased heat flow (Green *et al.*, 1997). A Palae-

ogene timing for dolomitization is attractive in the context of elevated heat flow associated with North Atlantic rifting and magmatism, and there is evidence of localized hydrothermal activity in the East Irish Sea Basin based on AFTA and vitrinite reflectance data (Cowan *et al.*, 1999; Holford *et al.*, 2005). However, associated fluid inclusions in late cements of Permo-Triassic reservoirs do not exceed 140°C (Hardman *et al.*, 1993). Moreover, there is no spatial relation between dolomite geobodies and Palaeogene

dykes on the Isle of Man. Furthermore, ankerite veins at Poyllvaaish are altered thermally where cross-cut by one such dyke.

Davies & Smith (2006) propose that a key characteristic of the 'hydrothermal dolomite play' is that alteration occurred at shallow depths and therefore early in the burial history of the host limestones. Mismatches between AFTA and vitrinite reflectance palaeothermometry in Carboniferous sections from the Irish Sea, Dublin and Navan basins has been used to argue for a Late Carboniferous palaeothermal episode (Green *et al.*, 1997; Corcoran & Clayton, 2001). A Mid–Late Carboniferous age for dolomitization on the Isle of Man is supported by evidence for elevated heat flow (eruption of the Scarlett Volcanics and local vitrinite reflectance data) but suffers from the lack of an identifiable source for high-salinity fluids. Carboniferous evaporites may be present offshore, but there is no direct evidence to suggest major thicknesses or proximal location. It has been shown above that hydrothermal fluids did not interact with the volcanics, and only one geobody is juxtaposed with them at outcrop.

In the Early Mesozoic, both the tectonic context (east–west extension) and the presence of thick evaporite strata as a hypersaline fluid source were satisfied, and elevated heat flow is likely to have accompanied East Irish Sea Basin rifting. However, the Mesozoic palaeothermal event is poorly constrained and variably masked by Palaeogene events. Early Cretaceous exhumation recorded by AFTA data from Carboniferous and Triassic strata resulted in cooling from temperatures up to 160°C, which have been attributed to deep burial rather than increased heat flow (Corcoran & Clayton, 2001). Other lines of evidence support a Mesozoic timing of fluid flow and dolomitization. Lead isotope model ages for Zn–Pb mineralization in the Manx Group give Variscan and Late Triassic/Early Jurassic ages (Crowley *et al.*, 1997a). Recently, hematite associated with Isle of Man mineralization has been palaeomagnetically dated to between *ca* 235 Ma and 245 Ma (Crowley *et al.*, 2013), as has hematite ore in the Manx Group at Maughold (associated with quartz and ferroan dolomite). In dolomite-hosted hematite veins and fault-related breccia cements in the Derbyhaven Formation near Cass-ny-Hawin, the hematite punctuates, and therefore is probably coeval with, DOL 3 cement (Figs 7E and F and 12B). Carbonate–sulphate–hematite fracture mineralization in Carboniferous limestones on the Cum-

brian coast, including abundant ferroan dolomite, has also been linked to fluids circulating out of the East Irish Sea Basin (Milodowski *et al.*, 1998).

Based on the foregoing discussion, a Triassic age for hydrothermal activity, dolomitization and Balladoole sphalerite mineralization is favoured (Table 1), with the proviso that the results imply a significant local (at least) perturbation in heat flow associated with regional rifting that has not been recognized previously. This perturbation may be due to later Cretaceous burial and/or Palaeogene heating annealing apatite fission tracks in the East Irish Sea Basin (e.g. Holford *et al.*, 2005). Discrepancy with the Pb model ages for Manx Group sulphide ore deposits may be indicative of multiple hydrothermal episodes associated with post-Variscan rifting, only one of which penetrated the limestones, owing to favourable timing of fault reactivation. This interpretation would broadly concur with complex fault-fracture-related mineralization recorded by Milodowski *et al.* (1998) on the eastern basin margin. Figure 19 depicts a conceptual model for cross-formational fluid flow associated with dolomitization during the Triassic.

Geobody size and distribution

Fault-fracture-related dolomites have been documented both at outcrop and subsurface, although in the latter case the geobody shapes and dimensions have to be interpolated from well data or rarely from 3D seismic imaging of associated porosity (e.g. Sagan & Hart, 2006). Wells are rarely drilled to intersect the key faults or damage zones, but stratigraphic discordance of paragenetically late replacive and saddle dolomites between adjacent boreholes is commonly taken as evidence of a fault-fracture control (e.g. Green & Mountjoy, 2005; Saller & Dickson, 2011). Presence of fractures or breccia within cores provides supporting evidence, as does the coincidence of seismically resolvable collapse features, sags, fault intersections or fault zones (Davies & Smith, 2006; Smith, 2006). However, subsurface geobodies can usually be mapped out only in onshore settings where tight grids of wells have been drilled. The giant Albion-Scipio hydrothermal dolomite petroleum field in the Ordovician Trenton-Black River play of the Michigan Basin is a classic example with wells drilled on a 20 acre grid (Hurley & Burdos, 1990). On a large scale, the Albion-Scipio dolomite occupies a narrow, elongate zone (*ca*
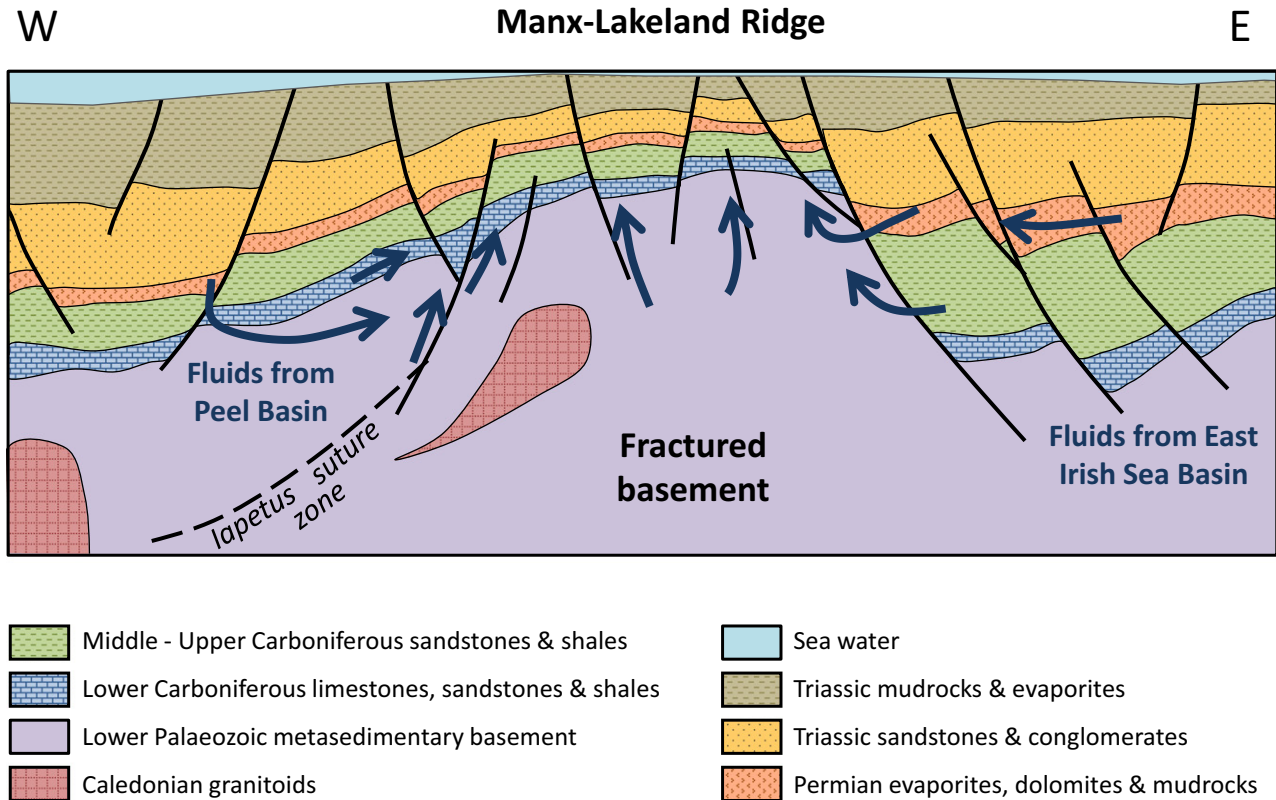
Fig 19. Conceptualized palaeohydrological interpretation for fault-related dolomitization showing basinal and basement-involved fluid sources that contributed to the hydrothermal circulation. Varying contributions from these sources through time, combined with differences in fluid flux, fluid–rock interaction and in mixing with resident pore fluids, produced the spatial heterogeneity in dolomite composition. Section is *ca* 50 km across.

1·2 km wide by 48 km long) but, in detail, it is highly variable in terms of lateral extension of individual geobodies away from major fault segments. Many outcrop examples of fault-fracture-related dolomite in extensional settings also combine to build a picture of elongate vertical sheet-like geobodies along the dominant tectonic discontinuities, but with lateral extensions that become increasingly stratabound at certain levels (sometimes called a 'Christmas tree' pattern). Some of the lateral 'branches' follow more coarsely textured or burrow-mottled limestones, suggesting a poroperm control on fluid migration, and others correspond to units with a dense mesh of interconnected joints or brecciation and porosity associated with karstification (e.g. Sharp *et al.*, 2010). Commonly, these branches exist beneath shale breaks in the succession, suggesting ponding of upward-percolating fluids beneath flow baffles (e.g. Grammer *et al.*, 2010; Grammer & Harrison, 2013).

The Isle of Man dolomite geobodies range from fracture-nucleated haloes of centimetre to deci-

metre width up to zones >300 m wide associated with major faults, and are typical of other outcropping examples (e.g. Zempolich & Hardie, 1997; Gasparrini *et al.*, 2006; Sharp *et al.*, 2010; Dewit *et al.*, 2012; Iriarte *et al.*, 2012; Martín-Martín *et al.*, 2012). Although the Isle of Man lacks extensive vertical exposure, field evidence suggests that grainy lithologies promoted lateral migration of dolomitizing fluids away from fault conduits. At a smaller scale, dolomite can locally be seen to exploit bed boundaries in muddy lithologies. An additional relation to DOL 1 distribution is less tangible, but impossible to rule out from the available data because no pervasive limestone replacement by DOL 1 has been found. Deep-seated fluids emplaced under pressure during fault activity will penetrate the relatively most permeable limestones. As the pressure drive dissipates, diffusion of introduced solutes along concentration gradients into resident pore fluids will still be permeability constrained. Although dolomitization cannibalizes limestones through dissolution–precipitation

reactions, it is difficult to envisage substantial lateral geobody development without the presence of effective pore networks in the host limestones. These may be residual primary porosity, diagenetic secondary porosity (including any related to earlier stratabound dolomitization events) or fracture and joint networks related to the fault damage zone. The latter may be a prerequisite where large geobodies develop in otherwise tight micritic limestone facies or late in the burial history when cementation has destroyed any residual limestone porosity. Otherwise, it would be reasonable to predict that large stratabound geobodies related to fault-fracture dolomitization form where the process takes place at shallow burial, for example, hydrothermal dolomitization in syn-rift carbonates associated with newly developing ocean basins (Wierzbicki *et al.*, 2006; Hollis *et al.*, 2012).

Fluid flow along tectonically active faults is episodic in nature due to strain cycling or seismic valving (Knipe, 1993; Muir-Wood, 1994; Eichhubl & Boles, 2000) and mass balance considerations require many such episodes in order to cause substantial dolomitization. Hydrothermal sulphide mineralization also requires pulsed, relatively rapid fluid flow in order to perturb the regional geothermal gradient (Gregg & Shelton, 2012). The presence of substantial breccia zones associated with the major faults in the study area support such a repetitive process (Philips, 1972; Sibson, 1987; Tarasewicz *et al.*, 2005; Iriarte *et al.*, 2012), rather than faults providing long-term 'passive' conduits owing to the prevailing *in situ* stress field. An implication is that permeability must be maintained or created with each increment of dolomitization in order for an areally large geobody to develop. It may be significant that dolomitization increases the mechanical rigidity of limestones, such that hydraulic microfracturing could potentially propagate along the dolomitic body as it develops. Such fractures could easily be obscured by subsequent dolomite precipitation. Alternatively, cooling hydrothermal fluids might result in dissolution of limestone in a 'halo' immediately outboard of the actively dolomitizing region in the manner proposed by Davies & Smith (2006). This is difficult to prove, because the only direct evidence of dissolution is in the rounded clasts in the fault-associated breccias (for example, Fig. 7C and E). In either case, it is probable that some residual interconnected porosity in the grainy facies of the Isle of Man limestones initially (at least) focused lateral fluid and solute migration away

from the main fault conduits. Hydrothermal alteration therefore probably took place prior to completion of deep burial cementation.

The fact that the largest geobody directly underlies the Bowland Shale calcareous mudrocks strongly supports the model of upward fluid migration. The mudrocks would have formed an aquiclude and a thermal insulator, facilitating lateral flow and precipitation of sphalerite and dolomite as the hydrothermal fluids cooled and mixed with resident pore waters (Shelton *et al.*, 2011). Ankerite veining in the Bowland Shale at Poyllvaaish may represent breaching of the aquitard seal and upward escape of the over-pressured mineralizing fluids. This suggestion is supported by the vein characteristics that are typical of tensile fractures (with a slight shear component) formed under elevated pore fluid pressure (Cosgrove, 1995), as well as by very high T_h and salinity values (Fig. 14) and the presence of minor sphalerite in the veins (Shelton *et al.*, 2011; Fig. 6C). Linear C-O isotope covariance with margin to centre ^{18}O depletion is peculiar to the veins (Fig. 15) and is difficult to explain by mixing thermally and compositionally distinct fluids. Alternative interpretations are CO_2 degassing or temperature-dependent isotopic fractionations with progressively increasing water–rock interaction (Zheng, 1990; Zheng & Hoefs, 1993). Both require ankerite precipitation from a CO_3^{2-} rich fluid, but the large range in T_h (87 to 288°C) and relatively modest spread in $\delta^{18}O$ (−11·4 to −15·3‰ VPDB) is easier to explain by degassing.

ECONOMIC IMPLICATIONS

Fault-fracture-related dolomite geobodies on the Isle of Man share many characteristics with structurally controlled hydrothermal dolomite reservoirs, as defined by Davies & Smith (2006), including tectonic control (with some evidence of hangingwall preference) breccias, abundant saddle dolomite with clear hydrothermal and hypersaline fluid-inclusion assemblages, isotopic signatures indicating evolved (high $\delta^{18}O$) basement-influenced (high $^{87}Sr/^{86}Sr$) fluids, and association with base metal sulphides. However, the Isle of Man dolomites have negligible matrix porosity and only localized, minor isolated vug porosity (mostly in breccia zones). They would not constitute a hydrocarbon reservoir in the subsurface. The lack of an effective porosity system is a function of: (i) the tightly interlocking

non-planar fabric of the dominant replacive DOL 2; (ii) over-dolomitization during DOL 2 formation augmented by abundant pore-filling DOL 3; (iii) the lack of a late stage dissolution episode (either dolomite dissolution or evidence for residual calcite that was leached after partial dolomitization); and (iv) the lack of major fracturing and brecciation events to rejuvenate poroperm subsequent to the completion of DOL 2 and DOL 3 precipitation (Gregg, 2004). In contrast, effective fault-fracture-related dolomite reservoirs commonly have planar matrix dolomite with intercrystalline porosity and/or connected vugs related to net volume reduction during limestone dolomitization and coeval or subsequent dissolution events (e.g. Smith, 2006; Weissenberger *et al.*, 2006). Dissolution may be a consequence of thermal or chemical disequilibrium between hydrothermal fluids and the limestones they invade, and also requires a means of exporting the dissolved carbonate (Esteban & Taberner, 2003; Machel, 2004).

As previously noted, formerly connected pore networks must have been present during dolomitization in order for the Isle of Man geobodies to attain their maximum size. The lack of preserved matrix porosity might therefore result from of a lack of hydrocarbon charge at an appropriate time to percolate into available pore space, reduce the effective water–rock ratio, and halt cementation. Fault-fracture-related dolomite reservoirs commonly contain hydrocarbon fluid inclusions within late stage void-filling cements. The same is true of gangue dolomite in many carbonate-hosted base metal sulphide deposits, reflecting the fact that the metal-bearing $CaCl_2$–$MgCl_2$–$NaCl$–H_2O brines are generated in and expelled from petroliferous sedimentary basins (Gregg & Shelton, 2012).

The north-western part of the East Irish Sea Basin closest to the Isle of Man is currently a gas (and oil) province, while the Peel Basin is sub-mature. Namurian prodelta shale source rocks contain mixed type II/III kerogens, but with dominant terrestrial type III. Cowan *et al.* (1999) ascribed hydrocarbon generation in the basin to post-Variscan rifting, elevated heat flow and rapid burial, such that the source rocks first entered the oil window in the Early Jurassic and the gas window in the Late Jurassic–Early Cretaceous. The relatively abundant gas charge displaced limited amounts of oil from initial traps below Middle Triassic evaporites, whereas leakier siliciclastic seal facies and relatively lower gas proportions allowed more oil to accumulate in the south of the basin. If hydrothermal fluid circulation took place in the Triassic, as argued above, it is unlikely that significant oil or gas would have reached the basin margin to become involved in the fault-fracture-related dolomitization processes.

Although the Isle of Man dolomites do not host hydrocarbons, they do act as the 'reservoir' for significant sphalerite mineralization at Balladoole. Shelton *et al.* (2011) discussed similarities of these ores to vein-hosted mineralization in the Manx Group, and minor amounts of sphalerite and galena have also been detected in veins cutting the Knockrushen Formation at Castletown. Bearing in mind the heterogeneity of isotopic and fluid-inclusion data among discrete dolomite geobodies, it is inferred that metaliferous hydrothermal brines circulating through the basement interacted to differing degrees with resident limestones and their fluids along different faults. In the case of the Balladoole Fault, conditions were suitable for mineralization, whereas a lesser supply of metals or greater dilution in other locations led to dolomite alone being formed. Fault-related dolomite and lead–zinc deposits in Carboniferous limestones are present around the margins of the Irish Sea, in North Wales, Eastern Ireland and Cumbria (cf. Wilkinson, 2003; Wilkinson *et al.*, 2005; Shelton *et al.*, 2011), and it is possible that the Isle of Man represents part of a spectrum of fluid–rock interaction scenarios related to the thermal, tectonic and hydrological evolution of the surrounding Mesozoic basins.

CONCLUSIONS

Viséan limestones from the south-eastern part of the Isle of Man contain numerous metre to hundreds of metre wide, fault-related and fracture-related bodies of ferroan dolomite. These bodies cross-cut stratigraphy and extend laterally away from tectonic conduits, particularly in grainstones. The largest geobodies are associated with major north-east/south-west faults that were probably basement structures that underwent extensional/transtensional reactivation in the Early Carboniferous and the Early Mesozoic. They have substantial zones of saddle dolomite-cemented dilatational breccias that record probable episodic hydraulic fracturing–cementation cycles. One of these zones, close to the Balladoole Fault, contains a dolomite-hosted sphalerite breccia deposit.

Replace planar-s to non-planar dolomite is pervasive within the geobodies and texturally destructive of all but the coarsest bioclasts. Breccia-hosted vugs, fractures and rare moulds are lined or filled by coarse ferroan saddle dolomite. Analogous ankeritic saddle dolomite is present in veins that cut the Bowland Shale Formation mudrocks, which stratigraphically overlie the largest dolomite geobody and Zn mineralization at Balladoole. These veins may represent escape of over-pressured fluid accompanying rupture of the mudrock aquitard during dolomitization and mineralization.

Dolomite isotope geochemistry and fluid-inclusion geothermometry constrain the nature of the palaeohydrological system, and document introduction of hydrothermal (≤292°C) post-evaporitic (≤24 wt% NaCl eq.) and lower salinity brines into the limestones. Both of these interacted with basement metasedimentary rocks and their more dilute host fluids, and the hypersaline brine probably originated in offshore salt-bearing sedimentary basins. Resultant dolomitizing fluids were emplaced episodically and co-seismically into the overlying limestones, but different fault conduits tapped different parts of the hydrothermal system, leading to subtle variations in the mineralogy and petrography within a consistent overall paragenesis. In addition, the fault and fracture conduits supported variable fluxes, and led to different rates of cooling and mixing with resident pore waters as well as differing degrees of water–rock interaction. This scenario is reflected in a range of dolomite compositions, temperatures and salinities that is neither geographically nor stratigraphically correlated.

The timing of hydrothermal activity and dolomitization remains equivocal, but an Early Mesozoic age is favoured. This affords the opportunity for Permo-Triassic strata in the East Irish Sea Basin to have supplied the evaporated sea water that is indicated by fluid-inclusion salinities. No regional thermal anomaly has been recorded for this time interval, but elevated geothermal gradients would be anticipated during rifting of the basin.

Despite bearing many of the hallmarks of a 'hydrothermal dolomite reservoir play' the Isle of Man dolomites are low porosity. This is because of predominantly non-planar dolomite fabrics, abundant dolomite cementation, a paucity of residual calcite within the geobodies for later leaching, the lack of a major fault brecciation event subsequent to the final void-filling dolomite cement, and the probable timing of dolomitization prior to oil expulsion from the kitchen areas in the East Irish Sea Basin.

ACKNOWLEDGEMENTS

REFERENCES

Bruckschen, P., **Oesmann, S.** and **Veizer, J.** (1999) Isotope stratigraphy of the European Carboniferous. Proxy signals for ocean chemistry, climate, and tectonics. *Chem. Geol.*, **161**, 127–163.

Chadwick, R.A., **Kirby, G.A.** and **Baily, H.E.** (1994) The post-Triassic structural evolution of north-west England and adjacent parts of the East Irish Sea. *Proc. Yorks. Geol. Polytech. Soc.*, **50**, 91–102.

Chadwick, R.A., **Jackson, D.I.**, **Barnes, R.P.**, **Kimbell, G.S.**, **Johnson, H.**, **Chiverrell, R.C.**, **Thomas, G.S.P.**, **Jones, N.S.**, **Riley, N.J.**, **Pickett, E.A.**, **Young, B.**, **Holliday, D.W.**, **Ball, D.F.**, **Molyneaux, S.G.**, **Long, D.**, **Power, G.M.** and **Roberts, D.H.** (2001) *Geology of the Isle of Man and its Offshore Area*. British Geological Survey Research Report, RR/01/06, 144 p.

Conliffe, J., **Azmy, K.**, **Gleeson, S.A.** and **Lavoie, D.** (2010) Fluids associated with hydrothermal dolomitization in St. George Group, western Newfoundland, Canada. *Geofluids*, **10**, 422–437.

Cope, J.C.W. (1997) The Mesozoic and Tertiary history of the Irish Sea. In: *Petroleum Geology of the Irish Sea and Adjacent Areas* (Eds N.S. Meadows, S.P. Trueblood, M. Hardman and G. Cowan), *Geol. Soc. London Spec. Publ.*, **124**, 47–59.

Corcoran, D.V. and **Clayton, G.** (2001) Interpretation of vitrinite reflectance profiles in sedimentary basins, onshore and offshore Ireland. In: *The Petroleum Exploration of Ireland's Offshore Basins* (Eds P.M. Shannon, P.D.W. Haughton and D.V. Corcoran), *Geol. Soc. London Spec. Publ.*, **188**, 61–90.

Cosgrove, J.W. (1995) The expression of hydraulic fracturing in rocks and sediments. In: *Fractography: Fracture Topography as a Tool in Fracture Mechanics and Stress Analysis* (Ed. M.S. Ameen), *Geol. Soc. London Spec. Publ.*, **92**, 187–196.

Cowan, G., **Burley, S.D.**, **Hoey, N.**, **Holloway, P.**, **Bermingham, P.**, **Beveridge, N.**, **Hamborg, M.** and **Sylta, Ø.** (1999) Oil and gas migration in the Sherwood Sandstone of the East Irish Sea Basin. In: *Petroleum Geology of Northwest Europe. Proceedings of the 5th Conference* (Eds A.J. Fleet and S.A.R. Boldy), pp. 1383–1398. Geological Society, London, Petroleum Geology Conference series.

Crowley, S.F, **Bottrell, S.H.** and **Haggerty, R.** (1997a) An isotopic investigation of base metal mineralization on the Isle of Man (IOM) and its relationship to fluid flow events and geotectonic evolution of the Irish Sea: initial results. In: *Geofluids II: Contributions to the Second International Conference on Fluid Evolution, Migration and Interaction in Sedimentary Basins and Orogenic Belts* (Eds J.P. Hendry, P.F. Carey, J. Parnell, A.H. Ruffell and R. Worden), pp. 319–322. The Queen's University of Belfast, Northern Ireland, UK.

Crowley, S.F., **Bottrell, S.H.**, **McCarthy, M.B.D.**, **Ward, J.** and **Young, B.** (1997b) $\delta^{34}S$ of Lower Carboniferous anhydrite, Cumbria, and its implications for barite mineralization in the northern Pennines. *J. Geol. Soc. London*, **154**, 597–600.

Crowley, S.F, **Piper, J.D.A.**, **Bamarouf, T.** and **Roberts, A.P.** (2013) Palaeomagnetic Evidence for the age of the Cumbrian and Manx hematite ore deposits: implications for the origin of hematite mineralization at the margins of the East Irish Sea basin, UK. *J. Geol. Soc. London*, **171**, 49–64.

Davies, G.R. and **Smith, L.B.** (2006) Structurally controlled hydrothermal dolomite reservoir facies: an overview. *Am. Assoc. Petrol. Geol. Bull.*, **90**, 1641–1690.

Dewit, J., **Huysmans, M.**, **Muchez, Ph.**, **Hunt, D.W.**, **Thurmond, J.B.**, **Vérges, J.**, **Saura, E.**, **Fernández, N.**, **Romaire, I.**, **Esetime, P.** and **Swennen, R.** (2012) Reservoir characteristics of fault-controlled hydrothermal dolomite bodies: Ramales Platform case study. In: *Advances in Carbonate Exploration and Reservoir Analysis* (Eds J. Garland, J.E. Nielson, S.E. Laubach and K.J. Whidden), *Geol. Soc. London Spec. Publ.*, **370**, 83–109.

Dickson, J.A.D. and **Barber, C.** (1976) Petrography, chemistry and origin of early diagenetic concretions in the Lower Carboniferous of the Isle of Man. *Sedimentology*, **23**, 189–211.

Dickson, J.A.D. and **Barber, C.** (1977) Chemical variation in a partially dolomitized Viséan limestone bed, Isle of Man. *Mineral. Mag.*, **41**, 145–153.

Dickson, J.A.D. and **Coleman, M.L.** (1980) Changes in carbon and oxygen isotope composition during limestone diagenesis. *Sedimentology*, **27**, 107–118.

Dickson, J.A.D., **Ford, T.D.** and **Swift, A.** (1987) The stratigraphy of the Carboniferous rocks around Castletown, Isle of Man. *Proc. Yorks. Geol. Soc.*, **46**, 203–229.

Eichhubl, P. and **Boles, J.R.** (2000) Rates of fluid flow in fault systems – evidence for episodic rapid fluid flow in the Miocene Monterery Formation, coastal California. *Am. J. Sci.*, **300**, 571–600.

Esteban, M. and **Taberner, C.** (2003) Secondary porosity development during late burial in carbonate reservoirs as a result of mixing and/or cooling of brines. *J. Geochem. Explor.*, **78–79**, 355–359.

Fitches, B. (2011) Tectonic structures in the Peel Sandstones and Carboniferous limestone, Isle of Man. *Geol. J.*, **46**, 364–373.

Fraser, A.J. and **Gawthorpe, R.L.** (2003) An Atlas of Carboniferous Basin Evolution in Northern England. *Geol. Soc. London Mem.*, **28**, 79.

Friedman, I. and **O'Neil, J.R.** (1977) Compilation of stable isotope fractionation factors of geochemical interest. In: *Data of Geochemistry* (Ed. M. Fleicher), *Geol. Surv. Prof. Pap.*, **440-KK**, KK1–KK12 + Figs.

Gasparrini, M., **Bechstädt, T.** and **Boni, M.** (2006) Massive hydrothermal dolomites in the southwestern Cantabrian Zone (Spain) and their relation to the Late Variscan evolution. *Mar. Petrol. Geol.*, **23**, 543–568.

Gawthorpe, R.L, **Gutteridge, P.** and **Leeder, M.R.** (1989) Late Devonian and Dinantian basin evolution in northern England and North Wales. In: *The Role of Tectonics in Devonian and Carboniferous Sedimentation in the British Isles* (Eds R.S. Arthurton, P. Gutteridge and S.C. Nolan), *Yorks. Geol. Soc. Occas. Publ.*, **6**, 1–23.

Goldsmith, J.R. and **Graf, D.L.** (1958) Structural and compositional variations in some natural dolomites. *J. Geol.*, **66**, 678–693.

Goldstein, R.J. and **Reynolds, T.H.** (1994) Systematics of fluid inclusions in diagenetic minerals. *SEPM Short Course*, **31**, 199.

Grammer, G.M. and **Harrison, W.B.** (2013) Evaluation and modeling of stratigraphic control on the distribution of hydrothermal dolomite away from major fault planes. RPSEA (Research Partnership to Secure Energy for America), Final Technical Report, Document Number 08123.12.Final, 997 pp.

Grammer, G.M., **Schulz, J.**, **Barnes, D.**, **Gillespie, R.**, **Harrison, W.B.** and **Thornton, J.E.** (2010) Stratigraphic Control on the Lateral Distribution of Hydrothermal Dolomites away from Major Fault Zones. American Association of Petroleum Geologists, Search and Discovery Article #50277 (http://www.searchanddiscovery.com/documents/2010/50277grammer/ndx_grammer.pdf)

Green, D.G. and **Mountjoy, E.W.** (2005) Fault and conduit controlled burial dolomitisation of the Devonian west-central Alberta Deep Basin. *Bull. Can. Petrol. Geol.*, **53**, 101–129.

Green, P.F., **Duddy, I.R.** and **Bray, R.J.** (1997) Variation in thermal history styles around the Irish Sea and adjacent areas: implications for hydrocarbon occurrence and tectonic evolution. In: *Petroleum Geology of the Irish Sea and Adjacent Areas* (Eds N.S. Meadows, S.P. Trueblood, M. Hardman and G. Cowan), *Geol. Soc. London Spec. Publ.*, **124**, 73–93.

Green, P.F., **Westaway, R.**, **Manning, D.A.C.** and **Younger, P.L.** (2012) Cenozoic cooling and denudation in the North Pennines (northern England, UK) constrained by apatite fission-track analysis of cuttings from the Eastgate Borehole. *Proc. Geol. Assoc.*, **123**, 450–463.

Gregg, J.M. (2004) Basin fluid flow, base-metal sulphide mineralization and the development of dolomite petroleum reservoirs. In: *The Geometry and Petrogenesis of Dolomite Hydrocarbon Reservoirs* (Eds C.J.R. Braithwaite, G. Rizzi and G. Darke), *Geol. Soc. London Spec. Publ.*, **235**, 157–175.

Gregg, J.M. and **Shelton, K.L.** (2012) Mississippi Valley-type mineralization and ore deposits in the Cambro-Ordovician Great American Carbonate Bank. In: *The Great American Carbonate Bank: The Geology and Economic Resources of*

the Cambro-Ordovician Sauk Megasequence of Laurentia (Eds J.R. Derby, R.D. Fritz, S.A. Longacre, W.A. Morgan and C.A. Sternach), *AAPG Mem.*, **98**, 163–186.

Grossman, E. (2012) Oxygen isotope stratigraphy, Chapter 10. In: *The Geological Time Scale 2012* (Eds F.M. Gradstein, J.G. Ogg, M. Schmitz and G. Ogg), pp. 181–206. Elsevier, Amsterdam.

Hardman, M., Buchanan, J., Herrington, P. and Carr, A. (1993) Geochemical modelling of the East Irish Sea Basin: its influence on predicting hydrocarbon type and quality. In: *Petroleum Geology of Northwest Europe. Proceedings of the 4th Conference* (Ed. J.R. Parker), pp. 809–821. Geological Society, London, Petroleum Geology Conference series.

Holford, S.P., Turner, J.P. and Green, P.F. (2005) Reconstructing the Mesozoic-Cenozoic exhumation history of the Irish Sea basin system using apatite fission track analysis and vitrinite reflectance data. In: *Petroleum Geology: North-West Europe and Global Perspectives – Proceedings of the 6th Petroleum Geology Conference* (Eds A.G. Doré and B.A. Vining), pp. 1095–1107. Geological Society, London, Petroleum Geology Conference series.

Hollis, C., Corlett, H., Hirani, J., Hodgetts, D., Gawthorpe, R.L., Rotevan, A. and Batesten, E. (2012) Fault/fracture related dolomitisation of the Eocene Thebes Formation, Hammam Fauran fault block, Gulf of Suez. American Association of Petroleum Geologists, Search and Discovery Article #50665 (http://www.searchanddiscovery.com/documents/2012/50665hollis/ndx_hollis.pdf)

Horita, J. (2005) Stable isotope thermometry: there is more to it than temperature. *Geochem. J.*, **39**, 481–496.

Hurley, N.F. and Burdos, R. (1990) Albion-Scipio and Stoney Point Fields-U.S.A. Michigan Basin. In: *Stratigraphic traps I* (Eds E.A. Beaumont and N.H. Foster), pp. 1–37. American Association of Petroleum Geologists, Treatise of Petroleum Geology, Atlas of Oil and Gas Fields, Tulsa, OK.

Iriarte, E., López-Horgue, M.A., Schroeder, S. and Caline, B. (2012) Interplay between fracturing and hydrothermal fluid flow in the Asón Valley hydrothermal dolomites (Basque-Cantabrian Basin, Spain). In: *Advances in Carbonate Exploration and Reservoir Analysis* (Eds J. Garland, J.E. Nielson, S.E. Laubach and K.J. Whidden), *Geol. Soc. London Spec. Publ.*, **370**, 207–227.

Jackson, D.I., Jones, N.S. and Waters, C.N. (2011) Irish Sea (including Kish Bank), Chapter 16. In: *A Revised Correlation of Carboniferous Rocks in the British Isles* (Eds C.N. Waters, I.D. Somerville, N.S. Jones, C.J. Cleal, J.D. Collinson, R.A. Waters, B.M. Besly, M.T. Dean, M.H. Stephenson, J.R. Davies, E.C. Freshney, D.I. Jackson, W.I. Mitchell, J.H. Powell, W.J. Barclay, M.A.E. Browne, B.E. Leveridge, S.L. Long and D. McLean), *Geol. Soc. Spec. Rep.*, **26**, 110–116.

Johnson, A.W., Shelton, K.L., Gregg, J.M., Somerville, I.D., Nagy, Z.R., Becker, S.P. and Wright, W.R. (2009) Regional studies of dolomites and their included fluids: recognizing multiple chemically distinct fluids during the complex diagenetic history of the Lower Carboniferous (Mississippian) rocks of the Irish Zn-Pb ore field. *Mineral. Petrol.*, **96**, 1–18.

Knipe, R.J. (1993) The influence of fault zone processes on fluid flow and diagenesis. In: *Diagenesis and Basin Development* (Eds A.D. Horbury and A.G. Robinson), *AAPG Stud. Geol.*, **36**, 135–154.

Lamplugh, G.W. (1903) *The Geology of the Isle of Man.* Memoir of the Geological Survey of England and Wales, 595 pp.

Land, L.S. (1980) The isotopic and trace element geochemistry of dolomite: the state of the art. In: *Concepts and Models of Dolomitization* (Eds D.H. Zenger, J.B. Dunham and R.L. Ethington), *SEPM Spec. Publ.*, **28**, 87–110.

Lapponi, F., Casini, G., Sharp, I., Blendinger, W., Fernández, N., Romaire, I. and Hunt, D. (2011) From outcrop to 3D modeling: a case study of a dolomitized carbonate reservoir, Zagros Mountains, Iran. *Petrol. Geosci.*, **17**, 283–307.

Laubach, S.E., Eichhubl, P., Hilgers, C. and Lander, R.H. (2010) Structural diagenesis. *J. Struct. Geol.*, **32**, 1866–1872.

Lavoie, D. and Chi, G. (2010) Lower Paleozoic foreland basins in eastern Canada: tectono-thermal events recorded by faults, fluids and hydrothermal dolomites. *Bull. Can. Petrol. Geol.*, **58**, 17–35.

Lonnee, J. and Machel, H.G. (2006) Pervasive dolomitization with subsequent hydrothermal alteration in the Clarke Lake gas field, Middle Devonian Slave Point Formation, British Columbia, Canada. *Am. Assoc. Petrol. Geol. Bull.*, **90**, 1739–1761.

López-Horgue, M.A., Iriarte, E., Schröder, S., Fernández-Mendiola, P.A., Caline, B., Corneyllie, H., Frémont, J., Sudrie, M. and Zerti, S. (2010) Structurally controlled hydrothermal dolomites in Albian carbonates of the Asón Valley, Basque Cantabrian Basin, Northern Spain. *Mar. Petrol. Geol.*, **27**, 1069–1092.

Machel, H.G. (2004) Concepts and models of dolomitization: a critical reappraisal. In: *The Geometry and Petrogenesis of Dolomite Hydrocarbon Reservoirs* (Eds C.J.R. Braithwaite, G. Rizzi and G. Darke), *Geol. Soc. London Spec. Publ.*, **235**, 7–63.

Machel, H.G. and Lonnee, J. (2002) Hydrothermal dolomite – a product of poor definition and imagination. *Sed. Geol.*, **152**, 163–171.

Maliva, R.G., Dickson, J.A.D. and Fallick, A.E. (1999) Kaolin cements in limestones: potential indicators of organic-rich pore waters during diagenesis. *J. Sed. Res.*, **69**, 158–163.

Martín-Martín, J.D., Gomez-Rivas, E., Travé, A., Salas, R. and Vergés, J. (2012) Dolomías controladas por fracturas en carbonatos aptienses de la zona de Benicàssim (SE Cuenca del Maestrat): distribución y características petrograficas. *Geogaceta*, **51**, 19–22.

Mazzullo, S.J. (1992) Geochemical and neomorphic alteration of dolomite: a review. *Carbonates Evaporites*, **7**, 21–37.

McArthur, J.M., Donovan, D.T., Thirlwall, M.F., Fouke, B.W. and Mattey, D. (2000) Strontium isotope profile of the early Toarcian (Jurassic) oceanic anoxic event, the duration of ammonite biozones, and belemnite palaeotemperatures. *Earth Planet. Sci. Lett.*, **179**, 269–285.

McArthur, J.M., Howarth, R.J. and Bailey, T.R. (2001) Strontium isotope stratigraphy: LOWESS version 3: Best fit to the marine Sr isotope curve for 0-509 Ma and accompanying look-up table for deriving numerical age. *J. Geol.*, **109**, 155–170.

Milodowski, A.E., Gillespie, M.R., Naden, J., Fortey, N.J., Shepherd, T.J., Pearce, J.M. and Metcalfe, R. (1998) The petrology and paragenesis of fracture mineralization in the Sellafield area, Cumbria. *Proc. Yorks. Geol. Soc.*, **52**, 215–241.

Muir-Wood, R.M. (1994) Earthquakes, strain-cycling and the mobilization of fluids. In: *Geofluids: Origin, Migration and*

Evolution of Fluids in Sedimentary Basins (Ed. J. Parnell), *Geol. Soc. London Spec. Publ.*, **78**, 85–98.

Needham, T. and **Morgan, R.** (1997) The East Irish Sea and adjacent basins: new faults or old? *J. Geol. Soc. London*, **154**, 145–150.

Newman, P.J. (1999) The geology and hydrocarbon potential of the Peel and Solway basins, East Irish Sea. *J. Petrol. Geol.*, **22**, 305–324.

Oliver, J. (1986) Fluids expelled tectonically from orogenic belts: the role in hydrocarbon migration and other geologic phenomena. *Geology*, **14**, 99–102.

Parnell, J. (1997) Fluid migration history in the north Irish Sea-North Channel region. In: *Petroleum Geology of the Irish Sea and Adjacent Areas* (Eds N.S. Meadows, S.P. Trueblood, M. Hardman and G. Cowan), *Geol. Soc. London Spec. Publ.*, **124**, 213–228.

Philips, W.J. (1972) Hydraulic fracturing and mineralization. *J. Geol. Soc. London*, **128**, 337–359.

Prokoph, A., **Shields, G.A.** and **Veizer, J.** (2008) Compilation and time series analysis of a marine carbonate $\delta^{18}O$, $\delta^{13}C$, $^{87}Sr/^{86}Sr$ and $\delta^{34}S$ database through Earth history. *Earth-Sci. Rev.*, **87**, 113–133.

Quirk, D.G. and **Kimbell, G.S.** (1997) Structural evolution of the Isle of Man and central part of the Irish Sea. In: *Petroleum Geology of the Irish Sea and Adjacent Areas* (Eds N.S. Meadows, S.P. Trueblood, M. Hardman and G. Cowan), *Geol. Soc. London Spec. Publ.*, **124**, 139–159.

Quirk, D.G., **Ford, D.T.**, **King, J.A.**, **Roberts, I.L.**, **Postance, R.B.** and **Odell, I.** (1990) Enigmatic boulders and syn-sedimentary faulting in the Carboniferous Limestone of the Isle of Man. *Proc. Yorks. Geol. Soc.*, **48**, 99–113.

Quirk, D.G., **Burnett, D.J.** and **Thomas, G.S.P.** (2006) The Castletown limestone. In: *A New History of the Isle of Man. Volume 1: The Evolution of the Natural Landscape* (Eds R.C. Chiverrell and G.S.P. Thomas), pp. 90–111. Liverpool University Press, Liverpool, UK.

Racey, A., **Goodall, J.G.S.** and **Quirk, D.G.** (1999) Palynological and geochemical analysis of Carboniferous borehole and outcrop samples from the Isle of Man. *J. Petrol. Geol.*, **22**, 349–362.

Ronchi, P., **Masetti, D.**, **Tassan, S.** and **Camocino, D.** (2012) Hydrothermal dolomitisation in platform and basin carbonate successions during thrusting: a hydrocarbon reservoir analogue (Mesozoic of Venetian Southern Alps, Italy). *Mar. Petrol. Geol.*, **29**, 68–89.

Rusk, B.G., **Lowers, H.A.** and **Reed, M.H.** (2008) Trace elements in hydrothermal quartz: relationships to cathodoluminescence and insights into vein formation. *Geology*, **36**, 547–550.

Sagan, J.A. and **Hart, B.S.** (2006) Three-dimensional seismic-based definition of fault-related porosity development: Trenton-Black River interval, Saybrook, Ohio. *AAPG Bull.*, **90**, 1763–1785.

Saller, A.H. and **Dickson, J.A.D.** (2011) Partial dolomitisation of a Pennsylvanian limestone buildup by hydrothermal fluids and its effect on reservoir quality and performance. *Am. Assoc. Petrol. Geol. Bull.*, **95**, 1745–1762.

Saunders, A.D., **Fitton, J.G.**, **Kerr, A.C.**, **Norry, M.J.** and **Kent, R.W.** (1997) The North Atlantic Igneous Province. In: *Large Igneous Provinces: Continental, Oceanic, and Planetary Flood Volcanism* (Eds J.J. Mahoney and M.F. Coffin), *Am. Geophys. Union Monogr.*, **100**, 45–94.

Sharp, I., **Gillespie, P.**, **Morsalnezhad, D.**, **Taberner, C.**, **Karpuz, R.**, **Vergés, J.**, **Horbury, A.**, **Pickard, N.**, **Garland, J.** and **Hunt, D.** (2010) Stratigraphic architecture and fracture-controlled dolomitisation of the Cretaceous Khami and Bangestan groups: an outcrop case study, Zagros Mountains, Iran. In: *Mesozoic and Cenozoic Carbonate Systems of the Mediterranean and the Middle East: Stratigraphic and Diagenetic Reference Models* (Eds F.S.P. Van Buchem, K.D. Gerdes and M. Esteban), *Geol. Soc. London Spec. Publ.*, **329**, 343–396.

Shelton, K.L., **Beasley, J.M.**, **Gregg, J.M.**, **Appold, M.S.**, **Crowley, S.F.**, **Hendry, J.P.** and **Somerville, I.D.** (2011) Evolution of a Carboniferous carbonate-hosted sphalerite breccia deposit, Isle of Man. *Miner. Deposita*, **46**, 859–880.

Sheppard, S.M.F. and **Gilg, H.A.** (1996) Stable isotope geochemistry of clay minerals. *Clay Miner.*, **31**, 1–24.

Sheppard, S.M.F. and **Schwarcz, H.P.** (1970) Fractionation of carbon and oxygen isotopes and magnesium between coexisting metamorphic calcite and dolomite. *Contrib. Miner. Petrol.*, **26**, 161–198.

Sibley, D. and **Gregg, J.M.** (1987) Classification of dolomite rock textures. *J. Sed. Res.*, **57**, 967–975.

Sibson, R.H. (1987) Earthquake rupturing as a mineralizing agent in hydrothermal systems. *Geology*, **15**, 701–704.

Sibson, R.H. (1994) Crustal stress, faulting and fluid flow. In: *Geofluids: Origin, Migration and Evolution of Fluids in Sedimentary Basins* (Ed. J. Parnell), *Geol. Soc. London Spec. Publ.*, **78**, 69–84.

Smith, L.B. (2006) Origin and reservoir characteristics of Upper Ordovician Trenton-Black River hydrothermal dolomite reservoirs in New York. *Am. Assoc. Petrol. Geol. Bull.*, **90**, 1691–1718.

Somerville, I.D. (2003) Review of Irish Lower Carboniferous (Mississippian) mud-mounds: depositional setting, biota, facies and evolution. In: *Permo-Carboniferous Carbonate Platforms and Reefs* (Eds W. Ahr, A.P. Harris, W.A. Morgan and I.D. Somerville), *SEPM Spec. Publ.*, **78**, and *AAPG Mem. 83*, 239–252.

Sweeney, J. and **Burnham, A.K.** (1990) Evaluation of a simple model of vitrinite reflectance based on chemical kinetics. *Am. Assoc. Petrol. Geol. Bull.*, **74**, 1559–1570.

Tarasewicz, J.P.T., **Woodcock, N.H.** and **Dickson, J.A.D.** (2005) Carbonate dilation breccias: examples from the damage zones to the Dent Fault, northwest England. *Geol. Soc. Am. Bull.*, **117**, 736–745.

Ward, J. (1997) Early Dinantian evaporites of the Easton-1 well, Solway Basin, onshore, Cumbria, England. In: *Petroleum Geology of the Irish Sea and Adjacent Areas* (Eds N.S. Meadows, S.P. Trueblood, M. Hardman and G. Cowan), *Geol. Soc. London Spec. Publ.*, **124**, 277–296.

Weissenberger, J.A.W., **Wierzbicki, R.A.** and **Harland, N.J.** (2006) Carbonate sequence stratigraphy and petroleum geology of the Jurassic Deep Panuke field, offshore Nova Scotia, Canada. In: *Giant Hydrocarbon Reservoirs of the World: From Rocks to Reservoir Characterization and Modelling* (Eds P.M. Harris and J.L. Weber), *AAPG Mem.*, **88**, 395–431.

Wendte, J., **Al-Aasm, I.S.**, **Chi, G.** and **Sargent, D.** (2009) Fault/fracture controlled hydrothermal dolomitization and associated diagenesis of the Upper Devonian Jean Marie Member (Redknife Formation) in the July Lake area of northeastern British Columbia. *Bull. Can. Petrol. Geol.*, **57**, 275–322.

Wierzbicki, R., **Dravis, J.J.**, **Al-Aasm, I.** and **Harland, N.** (2006) Burial dolomitization and dissolution of Upper Jurassic Abenaki platform carbonates, Deep Panuke reservoir, Nova Scotia, Canada. *Am. Assoc. Petrol. Geol. Bull.*, **90**, 1843–1861.

Wilkinson, J.J. (2003) On diagenesis, dolomitisation and mineralisation in the Irish-type Zn-Pb orefield. *Miner. Deposita*, **38**, 968–983.

Wilkinson, J.J., **Eyre, S.L.** and **Boyce, A.J.** (2005) Ore-forming processes in Irish-type carbonate-hosted Zn-Pb deposits: evidence from mineralogy, chemistry and isotopic compositions of sulfides at Lisheen Mine. *Econ. Geol.*, **100**, 63–86.

Woodcock, N.H. and **Barnes, R.P.** (1999) An early Ordovician turbidite system on the Gondwana margin: the southeastern Manx Group, Isle of Man. In: *In Sight of the Suture- the Palaeozoic Geology of the Isle of Man in its Iapetus Ocean Context* (Eds N.H. Woodcock, D.G. Quirk, W.R. Fitches and R.P. Barnes), *Geol. Soc. London Spec. Publ.*, **124**, 89–107.

Wright, W., **Johnson, A.W.**, **Shelton, K.L.**, **Somerville, I.D.** and **Gregg, J.M.** (2000) Fluid migration and rock interactions during dolomitisation of the Dinantian in Irish Midlands and Dublin Basin. *J. Geochem. Explor.*, **69–70**, 159–164.

Wright, W.R., **Somerville, I.D.**, **Gregg, J.M.**, **Shelton, K.L.** and **Johnson, A.W.** (2004) The Petrogenesis of dolomite, regional patterns of dolomitisation and fluid flow in the Lower Carboniferous of the Irish Midlands and Dublin Basin. In: *The Geometry and Petrogenesis of Dolomite Hydrocarbon Reservoirs* (Eds C.J.R. Braithwaite, G. Rizzi and G. Darke), *Geol. Soc. London Spec. Publ.*, **235**, 75–97.

Zempolich, W.G. and **Hardie, L.A.** (1997) Geometry of dolomite bodies within deep-water resedimented oolite of the Middle Jurassic Vajont Limestone, Venetian Alps, Italy: analogs for hydrocarbon reservoirs created through fault-related burial dolomitisation. In: *Reservoir Quality Prediction in Sandstones and Carbonates* (Eds J.A. Kupecz, J. Gluyas and S. Bloch), *AAPG Mem.*, **69**, 127–162.

Zhang, Y.G. and **Frantz, J.D.** (1989) Experimental determination of the compositional limits of immiscibility in the system $CaCl_2$–H_2O–CO_2 at high temperatures and pressures using synthetic fluid inclusions. *Chem. Geol.*, **74**, 289–308.

Zhang, L., **Liu, J.**, **Zhou, H.** and **Chen, Z.** (1989) Oxygen isotope fractionation in the quartz – water – salt system. *Econ. Geol.*, **84**, 1643–1650.

Zheng, Y.F. (1990) Carbon-oxygen isotopic covariation in hydrothermal calcite during degassing of CO_2: a quantitative evaluation and application to the Kushikino gold mining area in Japan. *Miner. Deposita*, **25**, 246–250.

Zheng, Y.F. and **Hoefs, J.** (1993) Carbon and oxygen isotopic covariations in hydrothermal calcites: theoretical modeling on mixing processes and application to Pb-Zn deposits in the Harz Mountains, Germany. *Miner. Deposita*, **28**, 79–89.

Supporting Information

Additional Supporting Information may be found in the online version of this article:

Appendix S1. Analytical methods. Details of sample preparation, analytical equipment and procedures.

Table S1. Localities, sample numbers and stratigraphic positions for dolomites and adjacent limestones collected and analysed in this study.

Table S2. Results of stable isotope analyses.

Table S3. Results of ICP-MS analyses

Figure S1. Additional fluid inclusion and C-O isotope cross-plots.

Figure S2. Vitrinite reflectance data from the study area.